MARCH 1979 LRP 149/79

DIAGNOSTICS OF A MAGNETIZED PLASMA BY REFLECTION OF GUIDED MICROWAVES

G. Cicconi[+], P.J. Paris

[+]Istituto di Elettrotecnica
dell'Universita di Genova, Italy

Diagnostics of a Magnetized Plasma

by Reflection of Guided Microwaves

G. Cicconi[+], P.J. Paris

Centre de Recherches en Physique des Plasmas
Ecole Polytechnique Fédérale de Lausanne

CH-1007 Lausanne / Switzerland

[+]Istituto di Elettrotecnica
dell'Universita di Genova, Italy

Abstract

Diagnostics of a magnetized plasma in presence of acoustic turbulence /1/ and of an ion acoustic test wave /2/ are presented and discussed.

From the values of the averaged electron density, measured by 30 GHz microwave interferometric unperturbative method, the reflection (and transmission) coefficient of a collisionless plasma cylinder in X band waveguide is computed by the Reflex numerical code /3/.

The experimental results of the amplitudes of the reflexion and transmission coefficients of the plasma, when the electric field vector is parallel to the magnetic field and in three different boundary conditions, are obtained as dependent on the discharge current and magnetic field intensity and compared with the calculation results. The equivalent radius of the column and the radial electron density distribution, which depend on the magnetic field are estimated for both homogeneous and parabolical profiles.

Both methods are compared as electromagnetic sensors of acoustic turbulence and ion acoustic test waves.

1. Introduction

Plasma diagnostics with microwaves are prevalently performed by applying transmission interferometric methods and by using microwave frequencies higher than the electron plasma frequency, where the plasma reflection is negligible. These methods are generally used to estimate the mean electron density of the plasma or also to detect its coherent or incoherent fluctuations /1/ /2/.

Nevertheless the measurement of the reflected microwave power from the plasma, which is important when the diagnostic frequency is below or near the electron plasma frequency, may yield additional data on the transversal distribution of the electron density and on collision processes through a cross correlation measurement between the transmitted and reflected waves.

Moreover,by lowering the diagnostic frequency which should be less expensive,one can use the reflexive interferometric method as a diagnostic tool.

In this report the results of reflexion-transmission experiments of guided microwaves through a low pressure plasma column of argon are presented and discussed. These results, obtained by three different waveguide couplings, are evaluated in order to gain experimental information to develop an unperturbative microwave diagnostic method. From the measurement of the reflection(or transmission) coefficient in waveguide, the plasma parameters are estimated by a numerical calculation.

The plasma column is created in a linear resistive discharge in a static magnetic field. The neutral gas pressure is 5.10^{-4} torr, and the plasma is considered as quiescient and collisionless /1/ /2/ (Fig. 1).

Two types of diagnostics are considered:

a) static, performed in a quiescient state of the plasma, where from the measured reflection and transmission coefficient mean electron density, the equivalent radius of the plasma column and a radial density profile are deduced from code calculation.

b) dynamic, performed in a given state of perturbation of the plasma, where the acoustic turbulence spectrum, driven by the discharge current, or the propagation properties of an ion acoustic test wave are measured.

The experimental results of the reflection-transmission method (RTX) are obtained by guided microwaves propagating in the dominant mode of a standard rectangular waveguide in X band (8 - 12 GHz) and are used to estimate the plasma parameters. The numerical code /3/ developed by an exact scattering theory in the waveguide is used to process the experimental results /5/ /6/. The radiation loss out of the waveguide due to a plasma column which transversally pierces the waveguide is neglected.

In the case a) the mean electron density value of the plasma column measured by a 30 GHz interferometer (MIR), is considered as valid and taken as a reference value to determine, through the RTX method, the equivalent plasma column radius and the electron density profile. The results are obtained as dependent on the discharge current and the axial magnetic field intensity. In the case b) the sensitivities of the RTX and MIR methods as electromagnetic sensors are determined and compared.

We used three microwave coupling devices, whose scattering characteristics were measured in the absence of plasma. They are the following:

a) an external conductor ring (ER), shown in Fig. 2, connects the input and the output (transmission port) waveguide on the external surface of the pyrex tube ($\sim$ 160 mm diam) where the plasma discharge is created. The design criteria of this device were strongly conditioned by the space available and limited by the presence of the magnetic field coils. In this case the ring, which has a diameter much greater than the plasma diameter, has high R-T losses and a high radiation loss with a very weak directivity. This device may be used for reflection ion measurements after a calibration of the reflectivity with a reference plasma since the Reflex code is not valid.

b) an inner large conductor tube (ILT), shown in Fig. 3, which connects the input and output waveguides, is placed in the interior of the pyrex tube. The tube diameter (60 mm) is greater than the waveguide width (22.86 mm) and slightly larger than the plasma diameter which does not exceed 50 mm. In this case the R-T loss is low and the radiation pattern of the tube has a good directivity. In this case the Reflex code may be used by taking into account a correction for the radiation loss.

c) the diameter of the plasma column is reduced to about 20 mm, less than the waveguide width, by an hollow ceramic disc placed on the cathode side. The waveguide is tapered as shown in Fig. 4 (IST). The radiation losses are weak and the Reflex code is used.

2. Theoretical Model

The geometry of the problem, in cylindrical coordinates, is shown in Fig. 5a /5/ /6/ /7/. The wave equation for the electric component of the electromagnetic field in the plasma column, assumed simple harmonic time dependence exp ($i\omega t$), is:

$$\frac{1}{r}\frac{\partial}{\partial r}\left(r\frac{\partial}{\partial r}E_p\right)+\frac{1}{r^2}\frac{\partial^2}{\partial\theta^2}E_p+k^2\varepsilon(\omega,r)E_p=0 \qquad (1)$$

The dielectric function $\varepsilon(\omega,r)$ is locally defined by assuming the electron density n as dependent of r:

$$\varepsilon(\omega,r)=1-\frac{1}{\omega(\omega-i\nu)}\cdot\frac{e^2}{\varepsilon_0 m}n(r) \qquad (2)$$

where υ is a global collision frequency considered as a constant. The electron density distribution over the cross section of the column is assumed to be parabolic in the form:

$$n(r)=N_0\left(1-\alpha\frac{r^2}{\rho^2}\right) \qquad (3)$$

where N_0 is the axial density, ρ the column radius and α a variable profile parameter with $0\leq\alpha\leq 1$.

Substituting (2) and (3) into (1), the radial part of this equation can be reduced to Whittaker's differential equation. The solution of this equation may be written, in terms of a Fourier series, as follows:

$$\begin{aligned}E_p(r,\theta)&=\sum_{m=0}^{\infty}A_m G_m(kr)\cos m\theta\\&=\sum_{m=0}^{\infty}A_m\exp\left[-i\frac{(\alpha\chi_0)^{1/2}}{2k\rho}(kr)^2\right]\cdot\left[\frac{i(\alpha\chi_0)^{1/2}}{k\rho}\right]^{\frac{m+1}{2}}(kr)^{m+1}\cdot\\&\cdot\phi\left(\frac{m+1}{2}+i\frac{h_0 k\rho}{4(\alpha\chi_0)^{1/2}},m+1;\frac{i(\alpha\chi_0)^{1/2}}{k\rho}(kr)^2\right)\cos m\theta \qquad (4)\end{aligned}$$

where $\chi_0=(e^2N_0)/(\varepsilon_0 m\omega(\omega-i\nu))$, $h_0=1-\chi_0$, $k=\frac{\omega}{c}$, and $\phi(a,b;r)$ is a confluent hypergeometric function also known as the Kummer function.

The electric field of the scattered waves in the rectangular waveguide by the plasma column, derived by applying the image principle (Fig. 5b), is:

$$E_s(r,\theta) = \sum_{m=0}^{\infty} B_m H_m^{(2)}(kr)\cos m\theta + \sum_{\pm}\sum_{m=0}^{\infty}\sum_{p=1}^{\infty}(-)^p B_m H_m^{(2)}\left(k r_p^{\pm}\right)\cos\theta_p^{\pm} \qquad (5)$$

where $(-)^p$ means that the wave reflexion occurs p times whereas its phase changes by $p\pi$, and $H_m^{(2)}(x)$ is the Hankel function.

The incident wave is assumed to be of TE (1,0) dominant mode, whose expression in cylindrical coordinates in given by the following Fourier expansion:

$$E_o(r,\theta) = \sum_{m=0}^{\infty} \varepsilon_m E_m J_m(kr)\cos m\theta$$

where $\varepsilon_o = 1$, $\varepsilon_m = 2$ $(m>0)$ is the Neumann factor,

$$E_{2m} = \cos 2m\varphi \quad , \quad E_{2m+1} = -i\sin(2m+1)\varphi$$

where $J_m(x)$ is the Bessel function, $\cos\varphi = \pi/ka$ where a is the waveguide width.

The coefficients B_m of the scattered waves are determined by solving the boundary-value problem along the surface of the plasma column. That is the tangential components of the electric and magnetic fields (or the normal derivative of the electric field) must be continous at the plasma surface. Hence an infinite set of linear equations for B_m is obtained:

$$B_{2s}F_{2s}(k_\rho) + \sum_{n=0}^{\infty}(-)^{n+s}B_{2n}\left[S_{2n+2s}(ka) + S_{2n-2s}(ka)\right] = -E_{2s},$$

$$B_{2s+1}F_{2s+1}(k_\rho) + \sum_{n=0}^{\infty}(-)^{n+s}B_{2n+1}\left[S_{2n+2s+1}(ka) + S_{2n-2s}(ka)\right] = -E_{2s+1} \qquad (7)$$

$$(s = 0,1,2,3\ldots\ldots\infty)$$

where $$S_n(ka) = \sum_{p=1}^{\infty} (-)^p H_n^{(2)}(pka)$$

is a Schlömilch series, and

$$F_n(k\rho) = \frac{1}{\varepsilon_n} \frac{G_n(k\rho) H_n^{(2)'}(k\rho) - G_n'(k\rho) H_n^{(2)}(k\rho)}{G_n(k\rho) J_n'(k\rho) - G_n'(k\rho) J_n(k\rho)}$$

The reflection and transmission coefficients are obtained by the asymptotic form of the scattered field E_s expressed in rectangular coordinates of the waveguide. One obtains /5/ /6/ :

$$E_s(y,z) \xrightarrow[z \to \pm\infty]{} \frac{1}{ak_o} \cos\frac{\pi}{a} x \sum_{m=0}^{\infty} (\mp)^m B_m E_m \exp(\mp i k_o z) \quad (8)$$

where $k_o = \sqrt{k^2 - \pi^2/a^2}$

The reflexion coefficient is then calculated as:

$$R(z) = \frac{1}{ak_o} \sum_{m=0}^{\infty} B_m E_m e^{2ik_o z} = |R| \exp[i(2k_o z + \theta)] \quad (9)$$

whose reference value, taken at z = 0, is

$$R(\theta) = |R| \exp(i\theta)$$

3. Experimental Results

In this section the experimental results obtained in the three coupling configurations are presented.

The microwave measurement apparatus is shown in Fig. 6 . The input microwave signal, in the band 8 - 10 GHz, is adjusted to a power level of 1 mW (0 dBm). The reflected power from the plasma is measured through a directional coupler by a power meter. The slide tuner matches the measurement device to the test set in the absence of plasma.

3. 1 MIR Method

This method, which is based on the use of a 30 GHz microwave horn interferometer, was applied in experiments described in /1/.

The electron density of the plasma versus discharge current, estimated by this method by considering the width of the plasma d = 5 cm is shown in Fig. 7. These results were used to calibrate the reflectivity in the ER experiment.

3. 2 External Ring, ER

This experiment is the simplest one. The device is schematically illustrated in Fig. 2. In this case the microwave generator is square-wave modulated at a frequency of 1 kHz and the reflected wave, from the plasma is detected by a standard microwave crystal detector.

In Fig. 8 the input characteristics of the device, measured in the absence of plasma, are shown in the whole waveguide band. The reflexion coefficient, in amplitude and phase, was determined by the VSWR (slotted guide measurement). By considering the device as a radiator, the estimation of the return loss gives P_L = (13-8) dB, as averaged in the band, where

$P_L = 10 \log_{10}(P_{inc} - P_{rad})/P_{inc} = 10 \log_{10}(P_{refl} + P_{trans})/P_{inc}$, with P_{inc}, P_{rad}, P_{refl} and P_{trans} are respectively the incident, radiated, reflected and transmitted powers. This device can be considered as a good radiator with bad directivity.

In Fig. 9 a the reflected power (diode voltage) is plotted versus the discharge current for a magnetic field intensity of 400 G (ν_c = 1120 MHz).

In Fig. 9 b a reference curve of the plasma electron density, measured by a 30 GHz horn interferometer (ref.1 par .3.2), is given versus the reflected power measured at the lowest frequency (8.15 GHz).

When, a current is drawn along in the axis of the device a turbulence spectrum /1/ is detected both in the reflection and transmission sides. The comparison between the spectrum display pictures, for current range 0-1 A, and those obtained by a Langmuir probe permits us to estimate that the probe sensitivity is about + 40 dB higher than the ER device sensitivity.

Moreover the signal detected by the cristals and fed into a lock-in amplifier was not able to resolve an ion-acoustic test wave, launched in the plasma by a grid. The same wave was detected by the 30 GHz horn interferometer.

Inner Large Tube, ILT

The device, used in this experiment, is shown in Fig. 3. In this case the output of the microwave generator is CW and the reflected and transmitted waves are detected by a bolometer system.

In Fig. 10 the input characteristics of the device, in the absence of the plasma, are plotted for the entire band. This device may be considered as a good radiator having a return loss $P_L = -(10 \div 12)$ dB and a radiation gain of the order of 15 dB.

In Figs. 11, 12, 13, the reflected and transmitted powers at 8.15, 8.90 and 9.35 GHz are plotted as dependent on the discharge current (0-3 A) and the axial magnetic field intensity (0.5 - 2.0 kG). The results at the frequency of 8.9 and 9.35 GHz (Figs 12 and 13) show a current dependent resonance (minimum of reflected and maximum of transmitted power) which appears at a lower current intensity when the magnetic field is

determined by the geometry of the copper tube which surrounds the plasma column.

The results at 8.15 GHz (Fig. 11) show no resonances. In this case, the copper tube, considered as a cylindrical waveguide section excited in TM 0,1 mode (λ_g = 5.4 cm) and connected to the rectangular waveguide, presents a short circuit on the large walls of the rectangular waveguides. These results may be used for the plasma diagnostic by the Reflex code.

The sensitivity of the ILT compared to a probe to the ion acoustic turbulence is -30 dB (reflection) and -40 dB (transmission).

In this case the lock-in system detected the ion acoustic wave launched in the plasma by means of a grid /2/. The measurements were carried out, in reflexion as well as in transmission, in the band 50 - 200 kHz. Wave patterns for 50 kHz are shown in Fig. 14. The resolution, in space, is of the order of 1.2 cm.

Inner Small Tube, IST

The waveguide used in this experiment is shown in Fig. 4. The waveguide is a low characteristic impedance waveguide (55 ohm) tapered at input and output to rectangular waveguides. The measurement conditions are as in the last case ILT. However in this case the plasma column was reduced in diameter by means of a ceramic shield as shown in Fig. 4.

In Fig. 15 the input characteristics of the waveguide, in the absence of plasma, are shown in the whole frequency band with (a) and without (b) the holes for the plasma column. This device can be considered as a bad radiator having an averaged P_L = (2 ÷ 3) dB in the band.

In Figs. 16, 17 and 18, the reflected (a) and the transmitted (b) powers at 8.2, 9.0, 10.0 GHz, are plotted as dependent on the discharge current (0-3 A) and the axial magnetic field intensity (0.5 - 2.0 kG).

The detection sensitivity of incoherent or coherent fluctuations was very poor (RTX/Probe $<$ .60 dB).

4. Calculation results

In order to estimate the plasma parameters from the experimental results, numerical calculations of the complex reflection coefficient (TE 1,0 mode), in X band standard rectangular waveguide by the Reflex code /3/ were carried out (Fig. 19).

The Reflex code results are made, without considering a vacuum sheath between plasma and walls, at a frequency of 8.15 GHz for the conditions of the ILT experiment. In Fig. 20 a the results are plotted along with the ILT experimental results in term of discharge current. One can see that a fit can be made by assuming that the radial electron density distribution tends to become flat when the magnetic field intensity is increased (optimum α = 0.7 (B = 0.5 kG) and α = 0.1 (B = 2 kG)). α is the inhomogeneity parameter $0 < \alpha < 1$ which depends on the electron density at the edge.

The Reflex code results at 9.0 GHz, are suitable to perform the fit with the experimental results of the IST experiment. In Fig. 20 b the results are drawn, in terms of reflectivity $/R/^2$ and discharge current, along with the experimental results. In this case, as in the ILT experiment, the optimal matching may be performed by considering that the radial electron density distribution becomes flat when the magnetic field intensity is increased. Moreover in the case of the weakest magnetic field (0.5 kG) a fitting is obtained only if the collisions are considered to be dominant (υ/ω = 1.0).

4. Discussion and Conclusions

In the last section we have shown the possibility to perform a graphical fit between the experiment and the calculated results of the Reflex code within a maximum deviation of the order of 15 %. For the reflectivity measurement in the set up shown in Fig. 6 a deviation of 10 % may be considered due to the matching of the experimental set up (/R/ = 0) without plasma. This value must be taken into account since the fit is performed without considering the phase of the reflection coefficient of the plasma, which is strongly altered by the matching operation /5/.

Moreover the theoretical model used for developing the Reflex code does not take into account the boundary conditions on the axis of the plasma column which is not considered as a plasma guide. Thus the electromagnetic model suits well the experiment when a fictitous microwave shortcircuit for the possible propagation modes, is assumed on the plasma sections of the rectangular waveguide large walls, in order to minimize the electromagnetic propagation into the plasma cylinder. In our case this condition may be considered approximately as satisfied at frequencies of 8.15 (ILT) and 9.0 GHz or at lower frequency (IST).

The fitting was essentially reached by considering the condition $\upsilon << \omega$ in the plasma dielectric permittivity equation except the IST case for B=0.5 kG), that is, a model of a collisionless plasma having a given radial electron density distribution. This hypothesis is equivalent to assuming the plasma column in the ambipolar diffusion regime as an extension of the Schottky theory for a low pressure plasma bounded by a conducting tube /7/. However the model described in /7/, in the presence of a longitudinal magnetic field, does not explain the radial electron density tendency to become flat, which corresponds to an enhanced diffusion coefficient when the magnetic field is increased.

In our case the result could be explained through the hypothesis of an enhancement of the plasma weak turbulence and the ionization degree /8/. However this diagnostic performed only by a graphical fit, could be yet developed by using a numerical and statistical method of fitting if more experimental data were available.

The microwave diagnostics presented here may be considered as a very valuable unperturbative method having an high sensitivity when the microwave diagnostic frequency is close to the value of the plasma frequency and suitable to investigate the electron density radial profile. These methods compared to the MIR set up have the advantage to be less expensive, because lower frequencies are used. A disadvantage is the use of a numerical code for the static diagnostic.

In the dynamic diagnostic of turbulence or test wave propagation, only the ILT experiment could be considered suitable to give a good result. The sensitivity is poor compared with the probe method however it is unperturbative. The ILT method could also be improved by replacing the copper tube with a longitudinal slotted tube in order to permit the grid, which launchs the test wave, to cross the tube over the whole length. And in order to increase the spatial resolution we could reduce, as in the case of IST, the E dimension of the waveguide.

Finally we have reached in these experiments three essentials results.

a) the measurement of microwaves using a very simple waveguide device can give information on density, density profile and effective collision frequency.

b) As a research result which gives us the possibility to develope a more suitable theoretical model for a magnetized plasma column, created by an RF discharge and accelerated by a static DC electric field.

c) To investigate the behaviour of the radial density profiles in the presence of instabilities.

5. Références

1) M. Bitter and P.J. Paris, Phys. Fluids 21 (4) p.609-616, April 1978.

2) P.J. Paris, M. Bitter and Ch. Hollenstein, Rev. Sci. Instrum. 48 (7) p.874-876, July 1977.

3) A.P. Benedetti and P. Poli, REFLEX, Comitato Nazionale Energia Nucleare CNEN, RT/FIMA (75) 3, (1975)

4) G. Cicconi, V. Molinari and C. Rosatelli, Jap. Journ. of Applied Physics, 12, 721, (1973)

5) G. Cicconi and C. Rosatelli, IEEE Trans. on Microwave Theory and Techniques, MIT-25, 11, 885, (1977)

6) H. Ikegami, Jap. Journ. of Applied Physics, 7, 6, p.634-655, (1968)

7) B.J. Bickerton and A. Von Engel, Proc. Phys. Soc. LXIX, 4-B, p.468, (1955)

8) H.B. Valentini, Proc. ICPIG, p.225, Berlin, (1977)

Acknowledgments

We would like to thank Prof. E.S. Weibel for making this collaboration possible.

The valuable discussions with Dr. Ch. Hollenstein and Dr. R.W. Means are gratefully acknowledged.

We like also to thank Dr. Paola Poli of the Centro di Calcolo of C.N.E.N. (Comitato Nazionale Energie Nucleare in Bologna (Italy) who supervised the numerical data processing.

Figure captions

Fig. 1 Experimental Device

Fig. 2 External Ring Device ER

Fig. 3 Inner large Tube Device ILT

Fig. 4 Inner Small Tube Device IST

Fig. 5 a) Geometry of the problem
b) Image principle

Fig. 6 Microwave set-up

Fig. 7 Density measurement by 30 GHz Interferometer (MIR method)

Fig. 8 Reflection coefficient $|R|$, output - input attenuation (dB), Reflection coefficient Phase Θ/Π versus frequency - for ER set-up

Fig. 9 Reflected voltage versus discharge current and frequency (ER set-up)
Electron density versus reflected voltage deduced from MIR measurement

Fig. 10 Reflection coefficient $|R|$, output - input attenuation (dB), Reflection coefficient Phase $\frac{\Theta}{\Pi}$ versus frequency - for ILT set-up

Fig. 11 Reflected and Transmitted Power versus discharge current for 8.15 GHz - ILT set-up

Fig. 12 Idem for 8.90 GHz

Fig. 13 Idem for 9.35 GHz

Fig. 14 Detection of ion acoustic test wave (50 kHz) on reflection and transmission arm of the microwave set-up - for ILT set-up

Fig. 15 Reflection coefficient $|R|$, output-input attenuation (dB), Reflection coefficient Phase $\frac{\Theta}{\Pi}$ versus frequency - for IST set-up

Fig. 16 Reflected and Transmitted Power versus discharge current for 8.2 GHz - IST set-up

Fig. 17 Idem for 9.0 GHz

Fig. 18 Idem for 10.8 GHz

Fig. 19 Reflection coefficient amplitude $|R|$ and Phase $\frac{\Theta}{\Pi}$ vs. Plasma electron density caculated at 8.5 GHz for $\frac{\nu}{\omega} = 0.0$ and 0.05, $\rho_o = 15.4$ mm and $\rho_1 = 12.5$, 10.0 and 7.54 mm ($\alpha = 10^{-5}$)

Fig. 20 a) Reflectivity $|R|^2$ calculated along with the experimental points versus discharge current for 8.15 GHz - ILT set-up

b) Reflectivity $|R|^2$ calculated along with the experimental data versus discharge current for 9.0 GHz - IST set-up

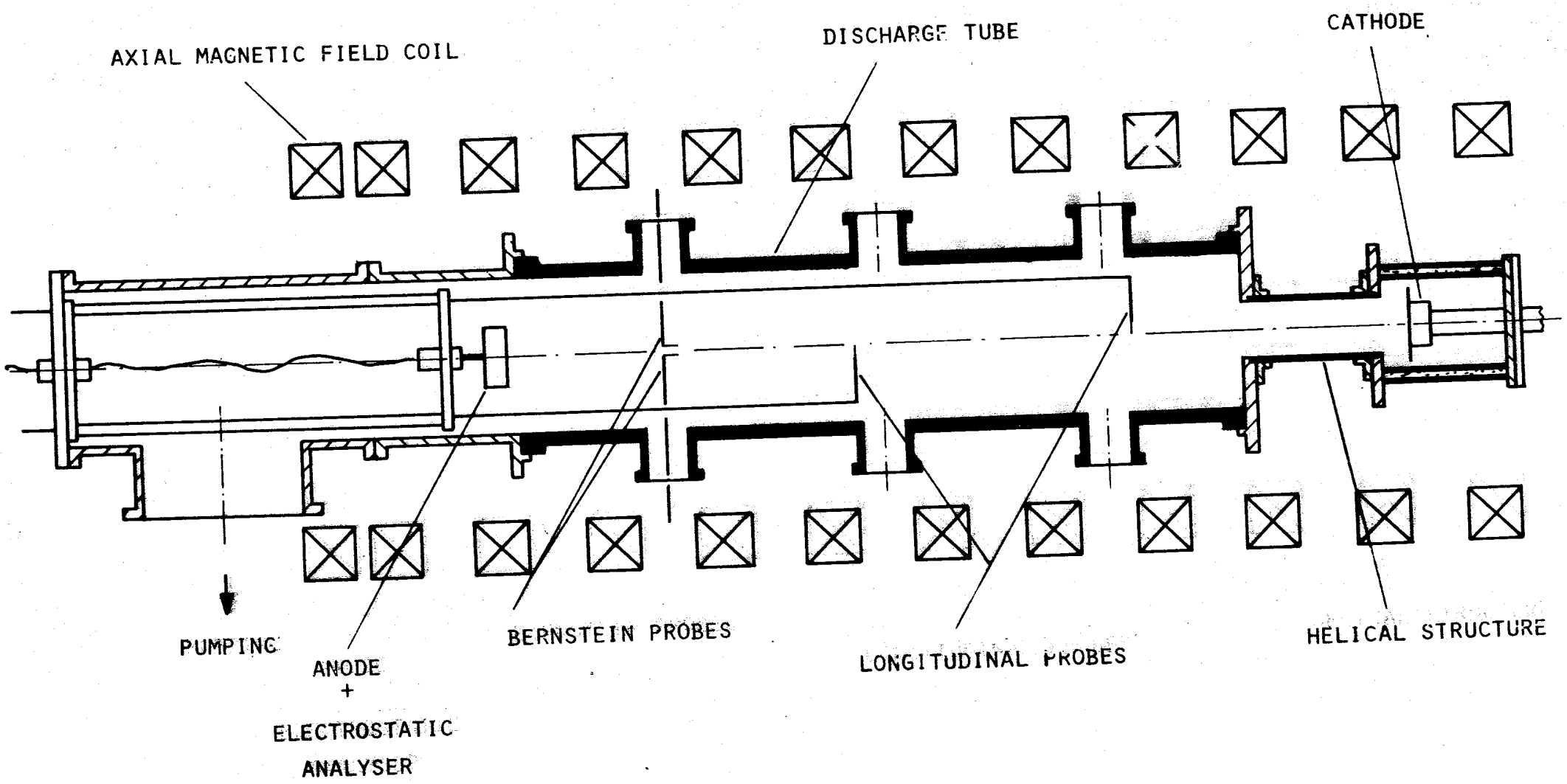
AXIAL MAGNETIC FIELD COIL
DISCHARGE TUBE
CATHODE
PUMPING
ANODE
+
ELECTROSTATIC
ANALYSER
BERNSTEIN PROBES
LONGITUDINAL PROBES
HELICAL STRUCTURE

FIG 1

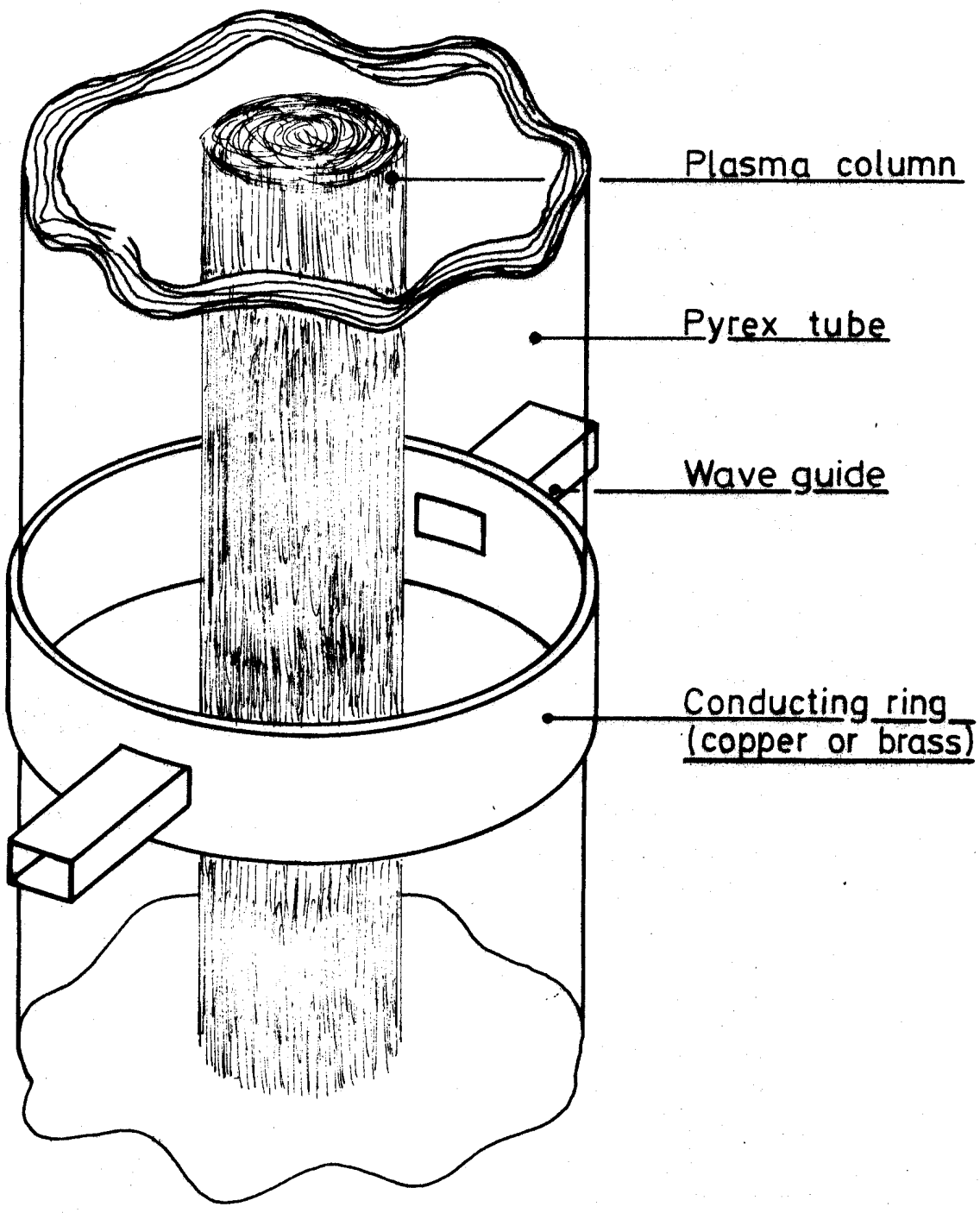

Structure ER

Fig 2

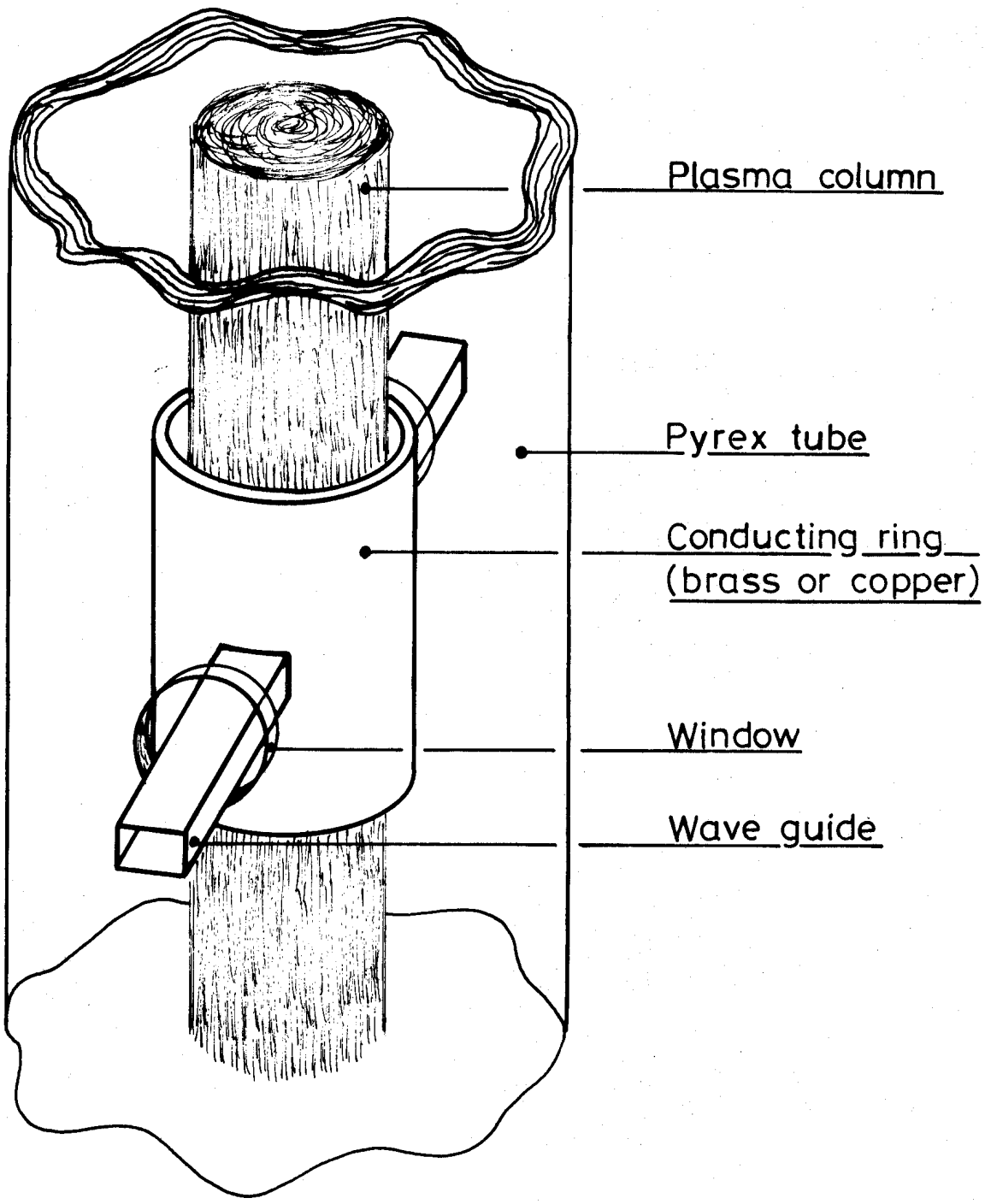

Structure ILT

Fig 3

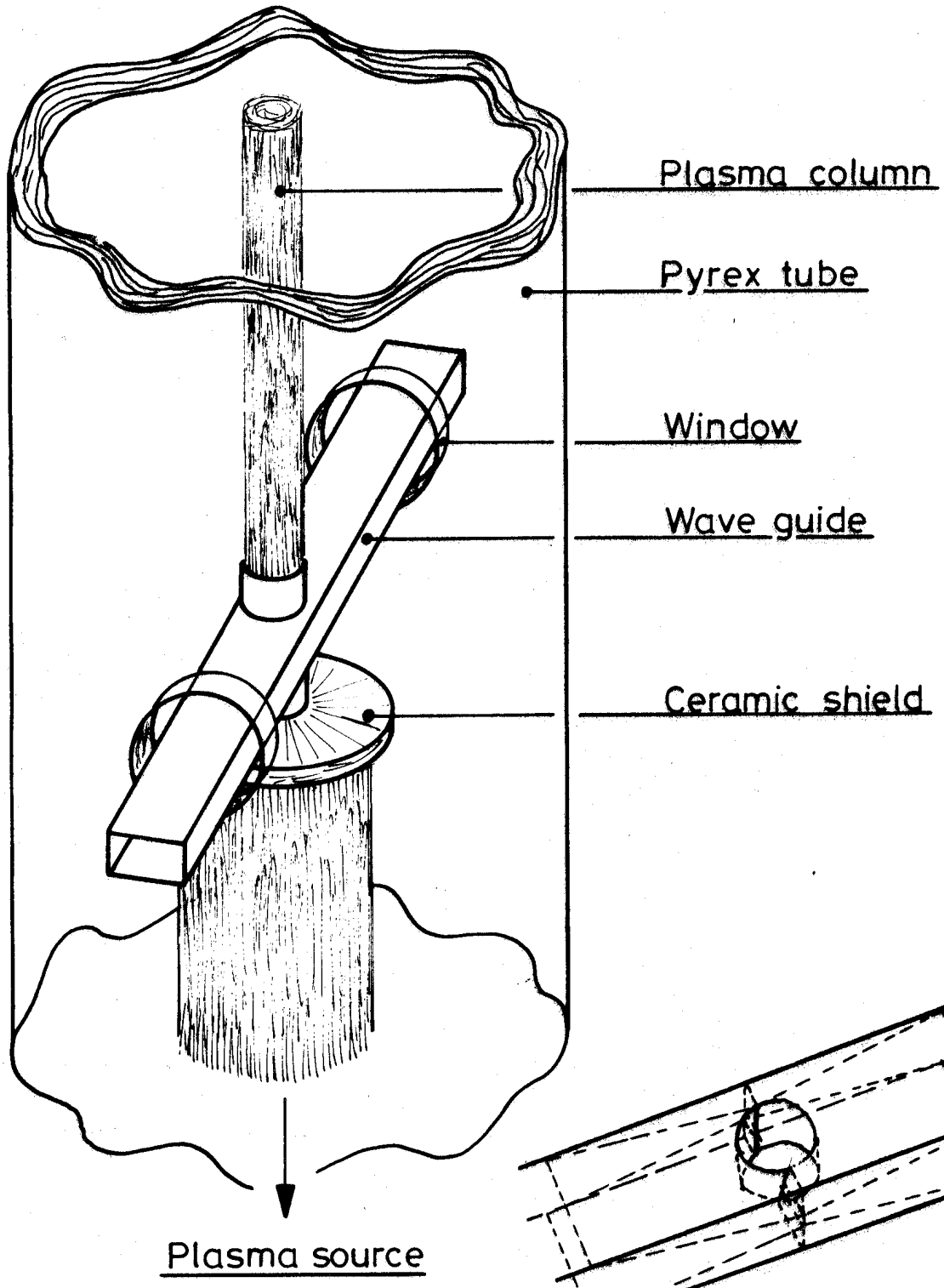

Structure IST

DETAIL OF
THE TAPPERED WAVEGUIDE

Fig 4

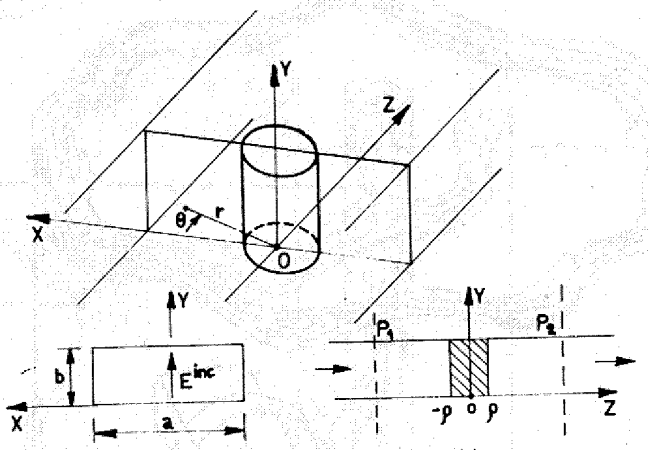

Fig. 1. The geometry of the problem.

A)

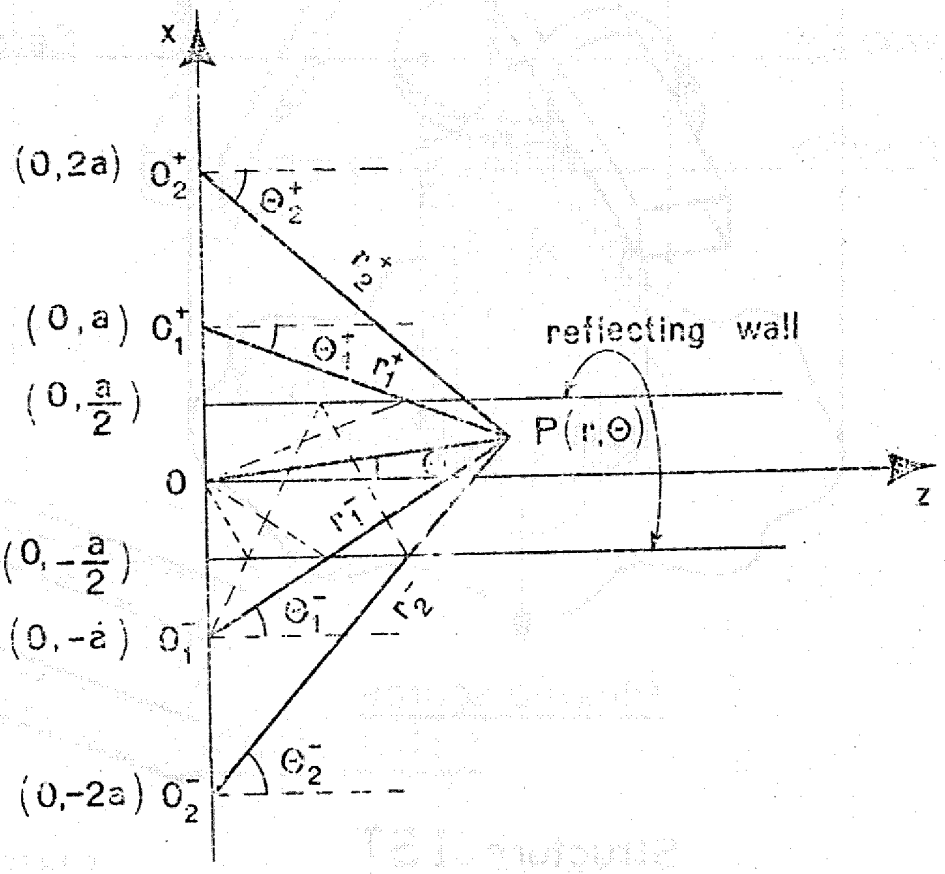

B)

FIG 5

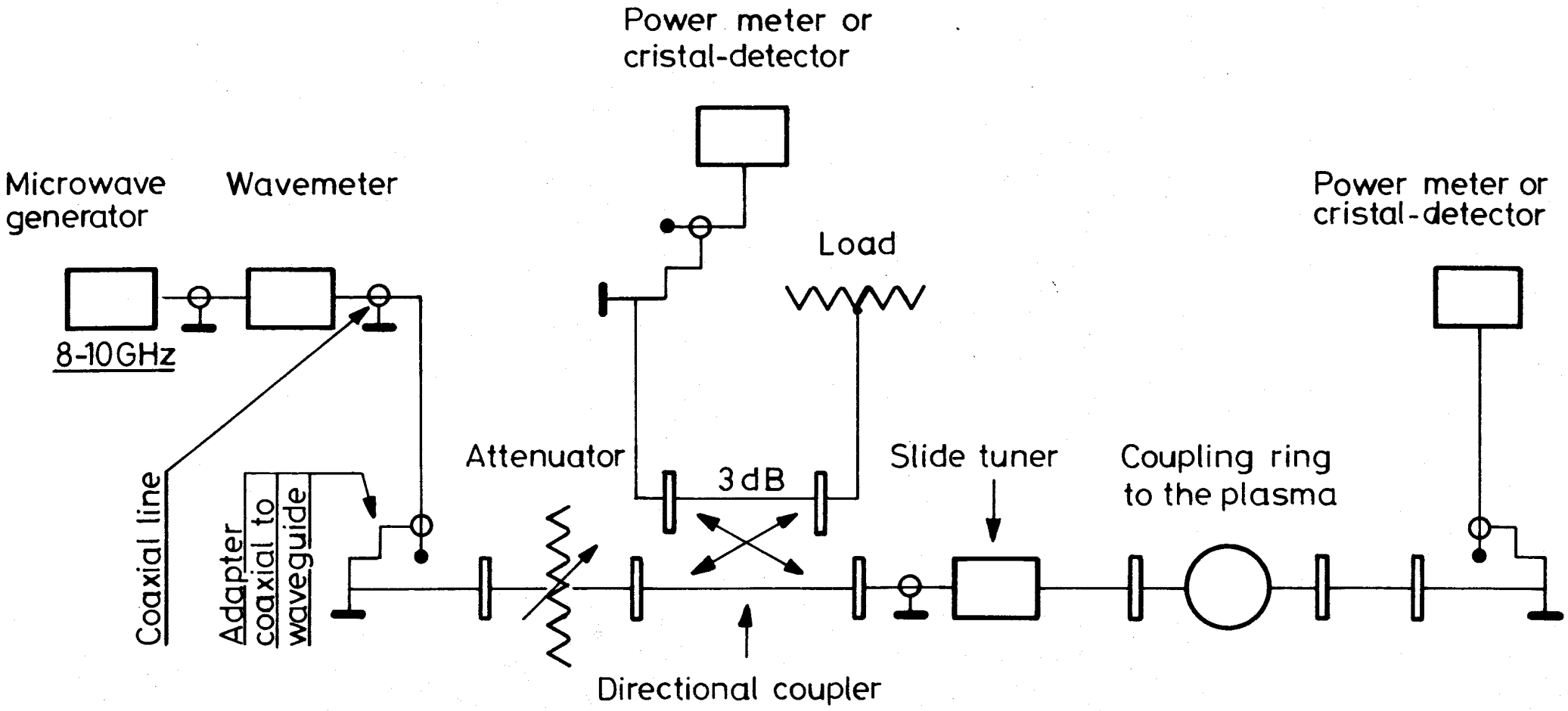

Fig 6 Experimental set-up

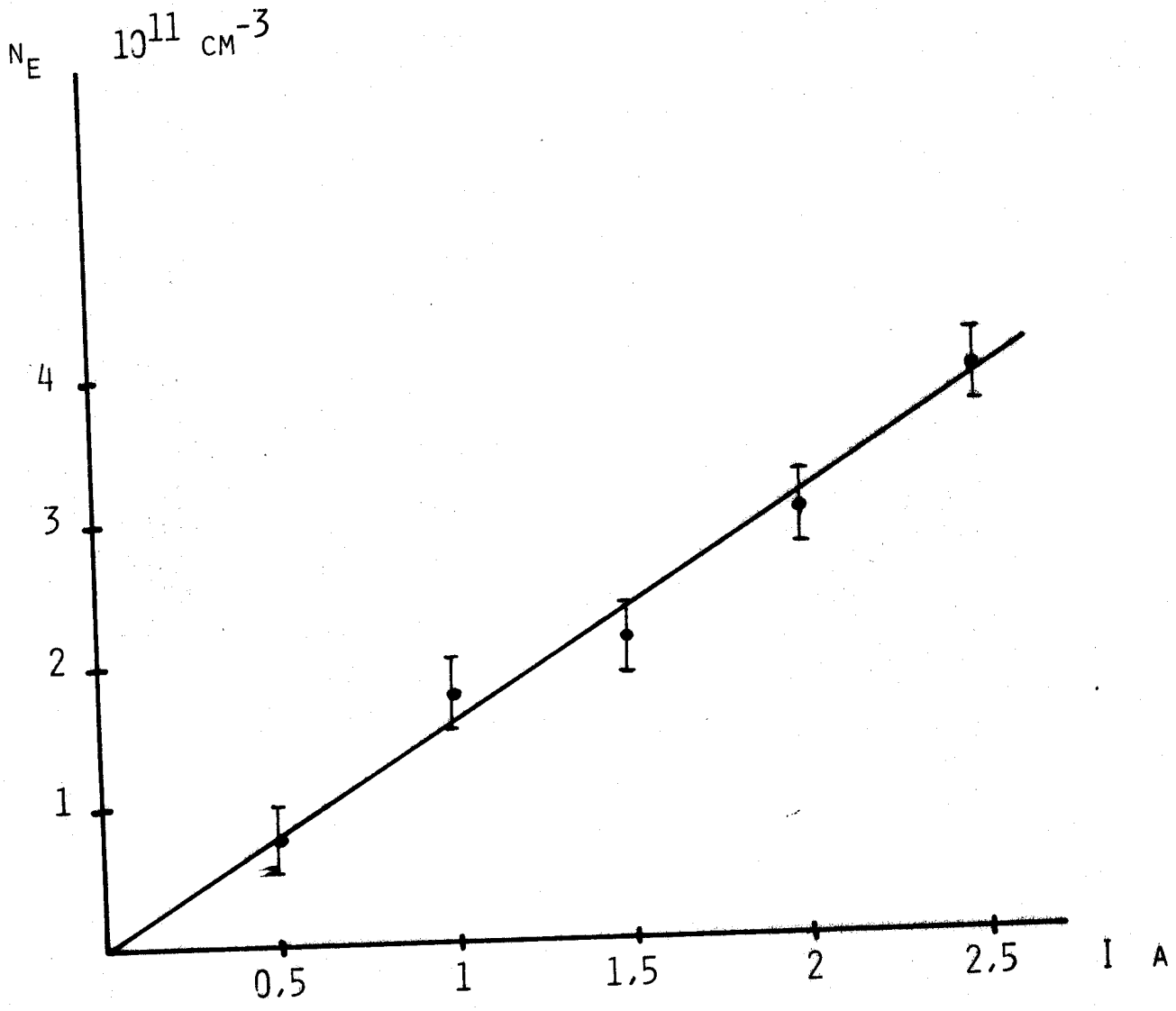

Electron density measurement with
the 30 GHz Interferometer

FIG 7

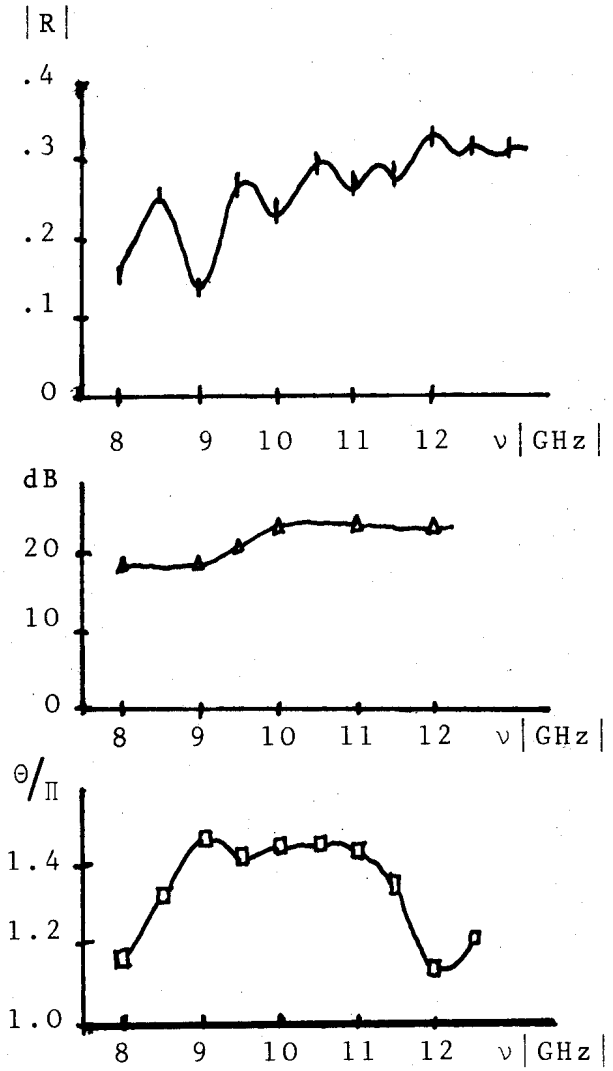

Reflection, attenuation and reflection Phase coefficients versus Frequency for ER Set-up

FIG 8

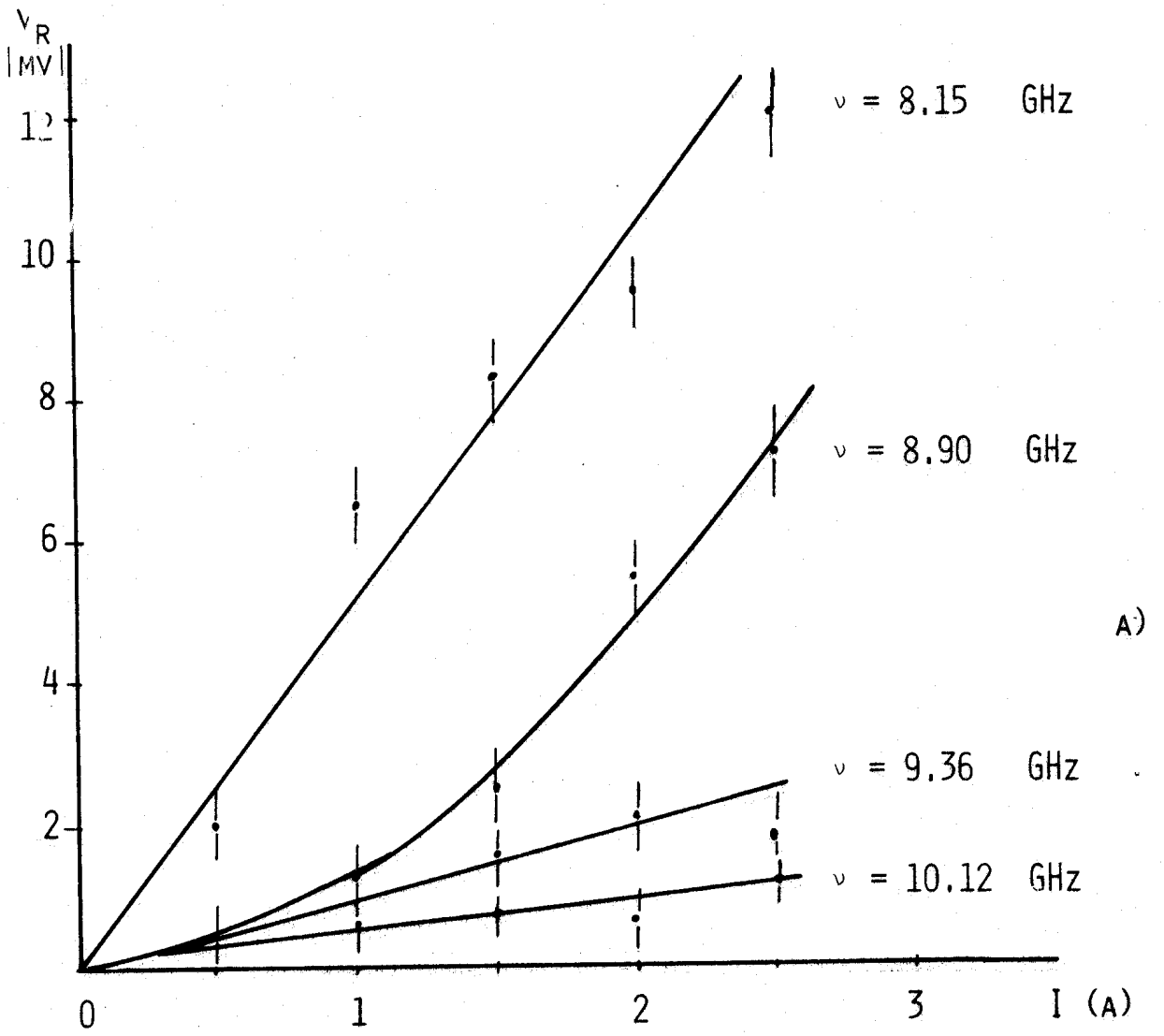
V_R |MV|
12
10
8
6
4
2
0
1
2
3
I (A)
ν = 8.15 GHz
ν = 8.90 GHz
ν = 9.36 GHz
ν = 10.12 GHz
A)

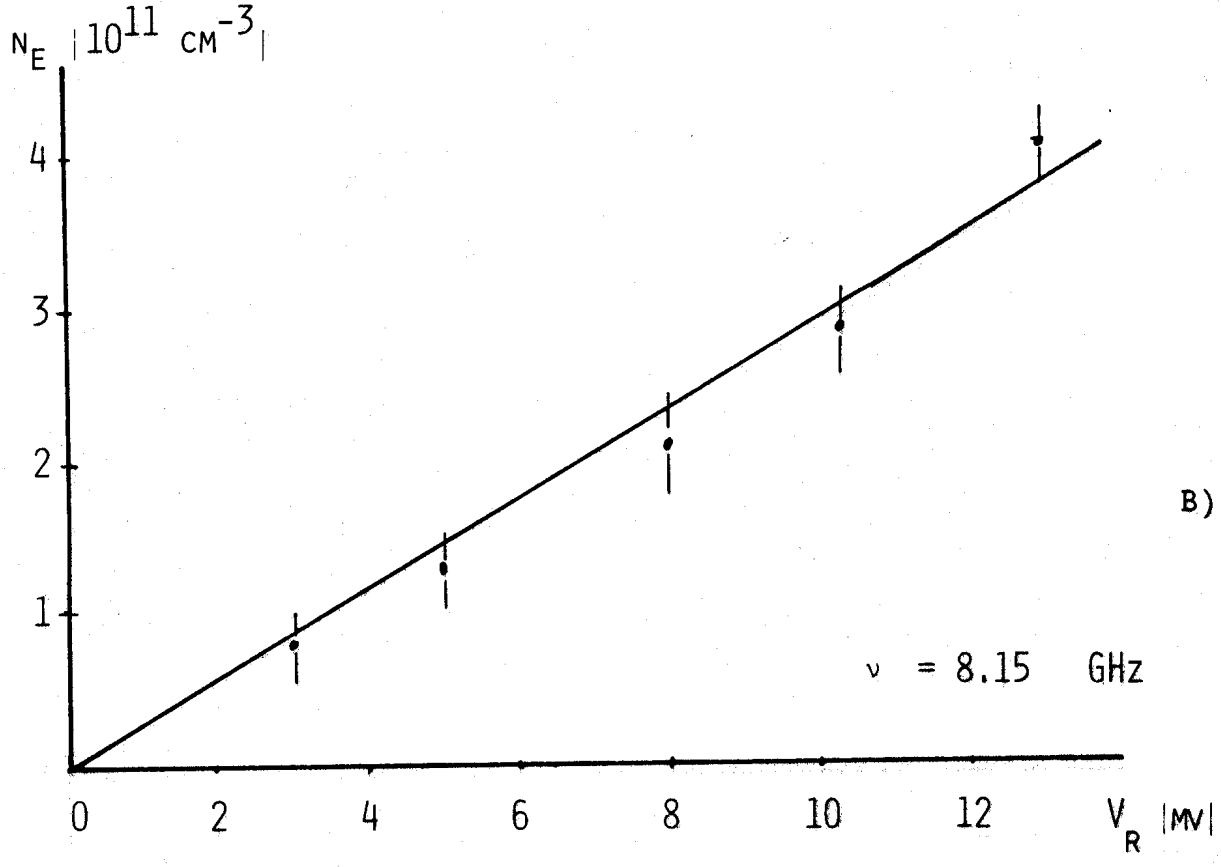
N_E |10^{11} cm^{-3}|
4
3
2
1
0
2
4
6
8
10
12
V_R |MV|
ν = 8.15 GHz
B)

FIG 9

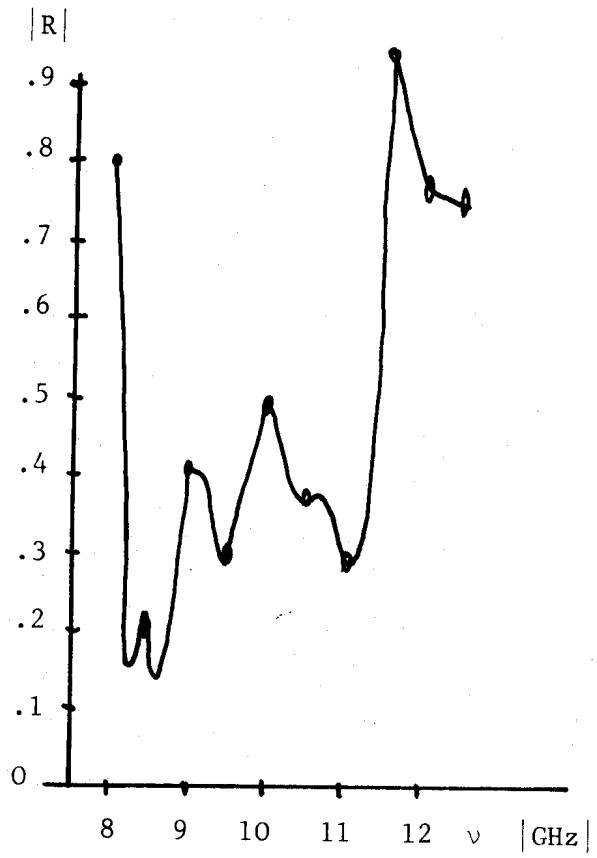

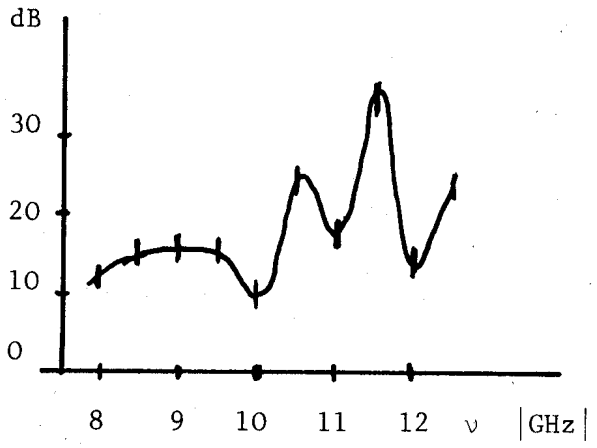

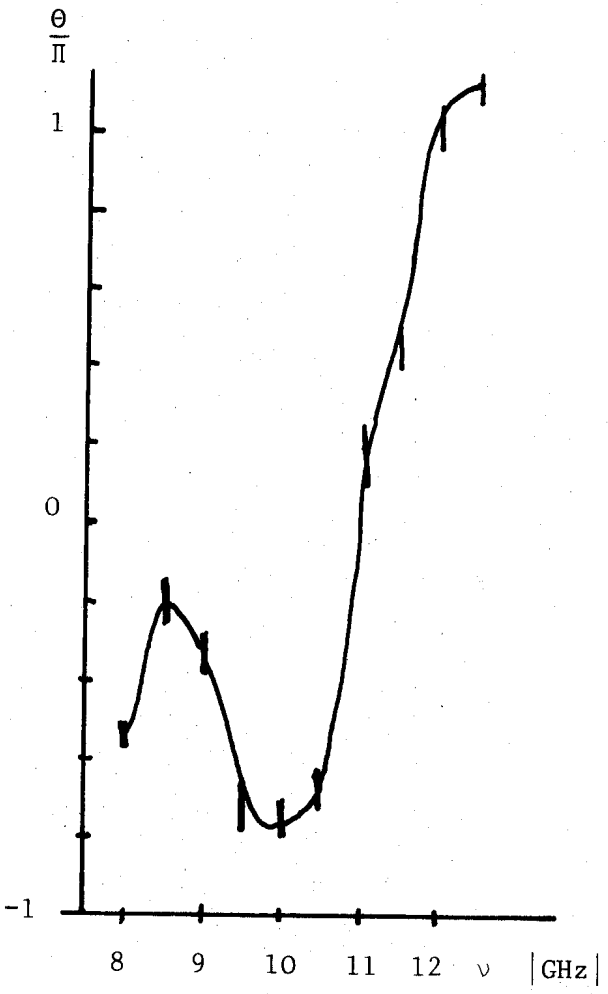

Reflection, attenuation and reflection Phase coefficients versus Frequency for ILT Set-up

FIG 10

ν = 8.15 GHz

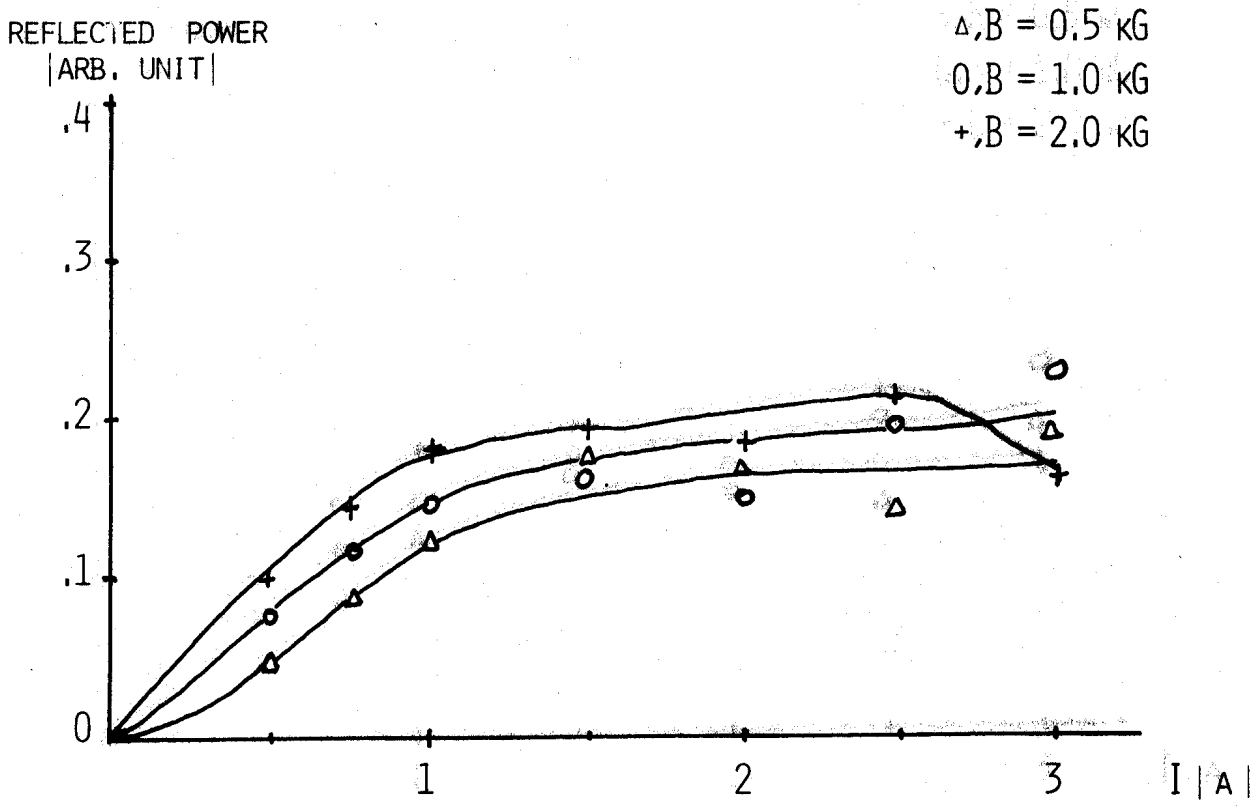

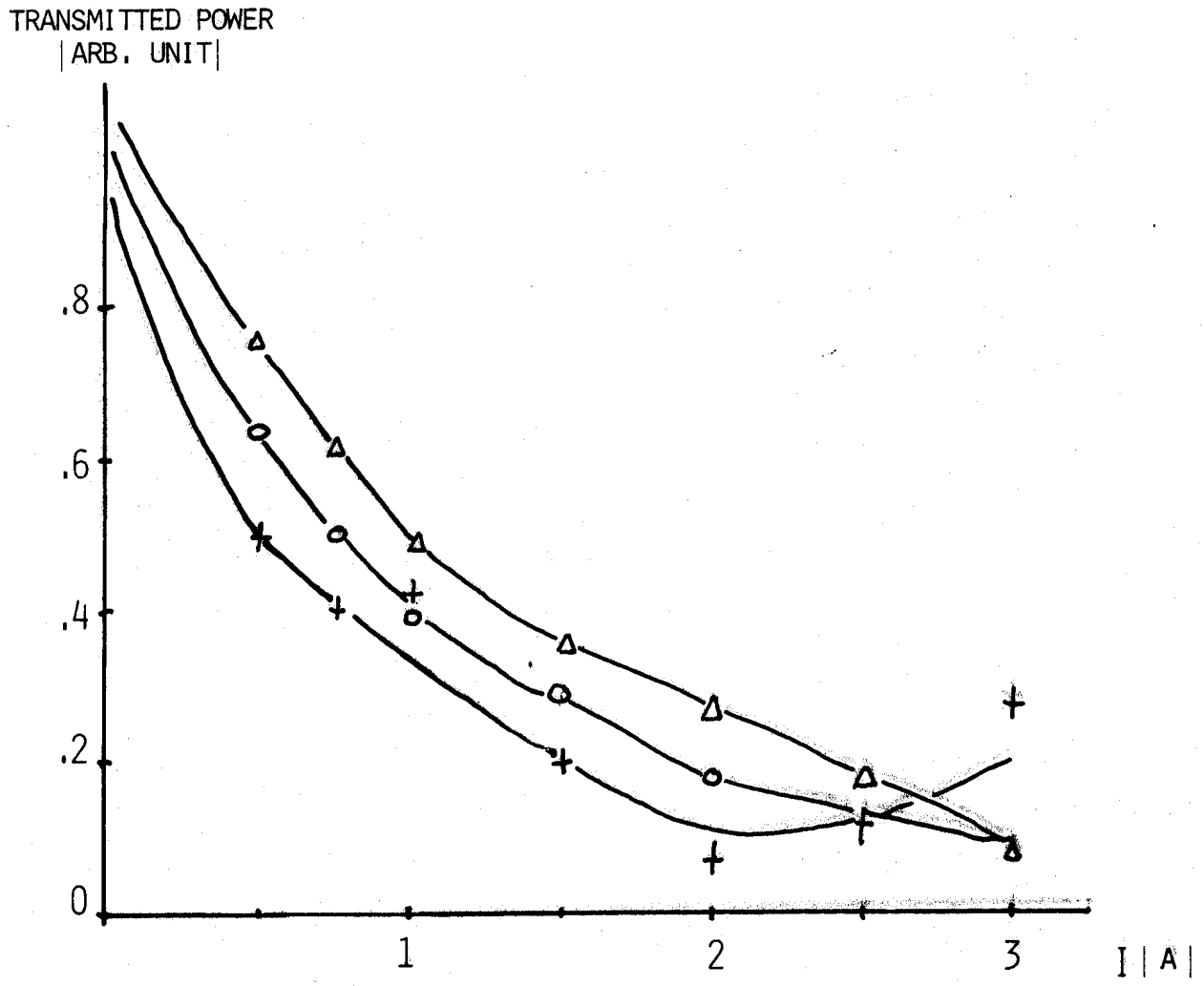

FIG 11

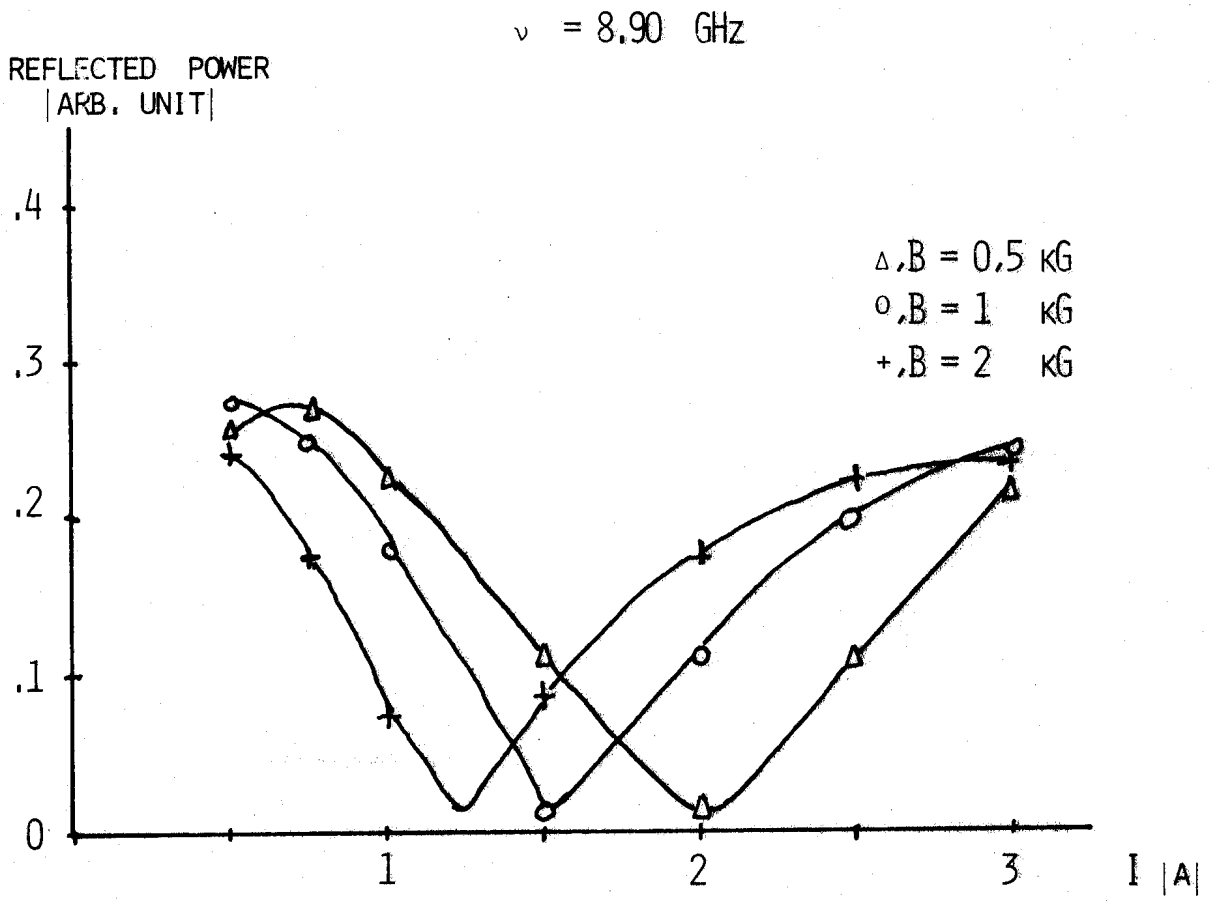
ν = 8.90 GHz
REFLECTED POWER
|ARB. UNIT|
.4
.3
.2
.1
0
Δ, B = 0,5 KG
o, B = 1 KG
+, B = 2 KG
1
2
3
I |A|

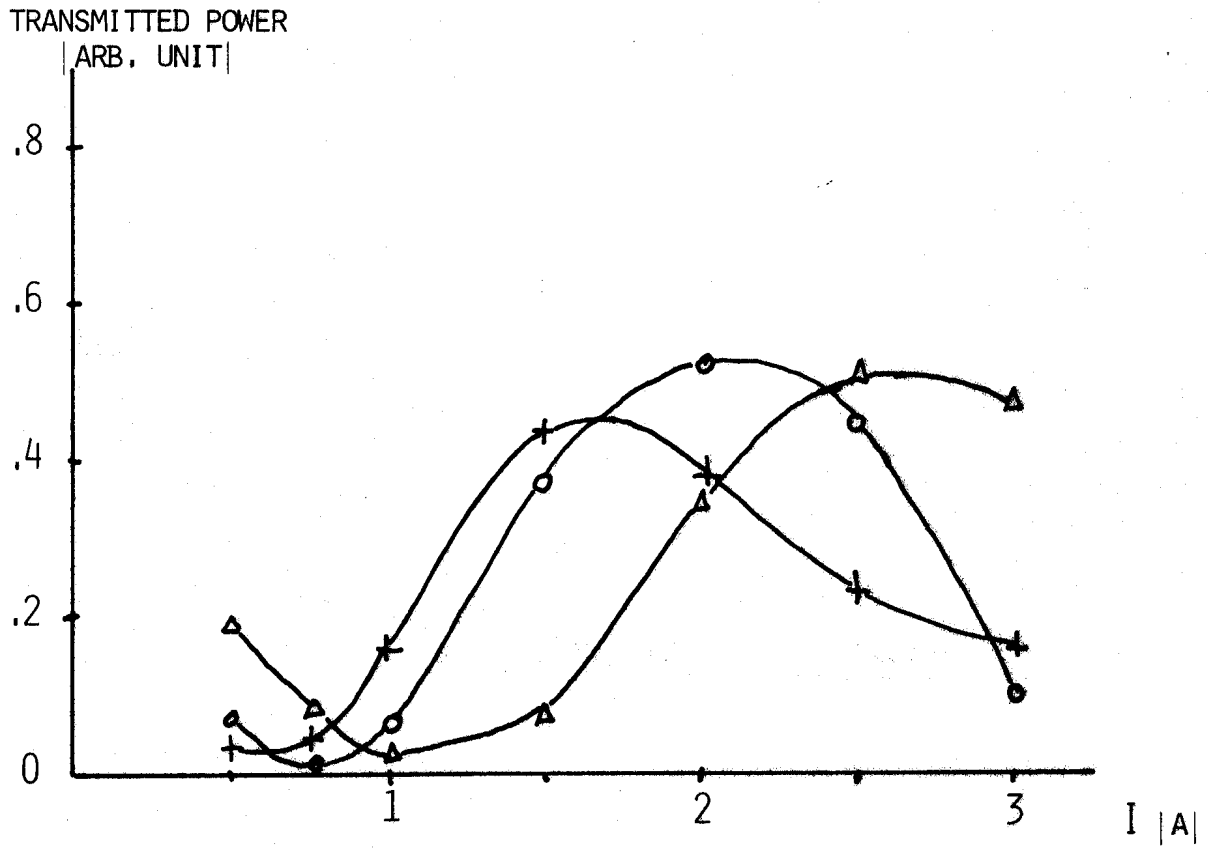
TRANSMITTED POWER
|ARB. UNIT|
.8
.6
.4
.2
0
1
2
3
I |A|

FIG 12

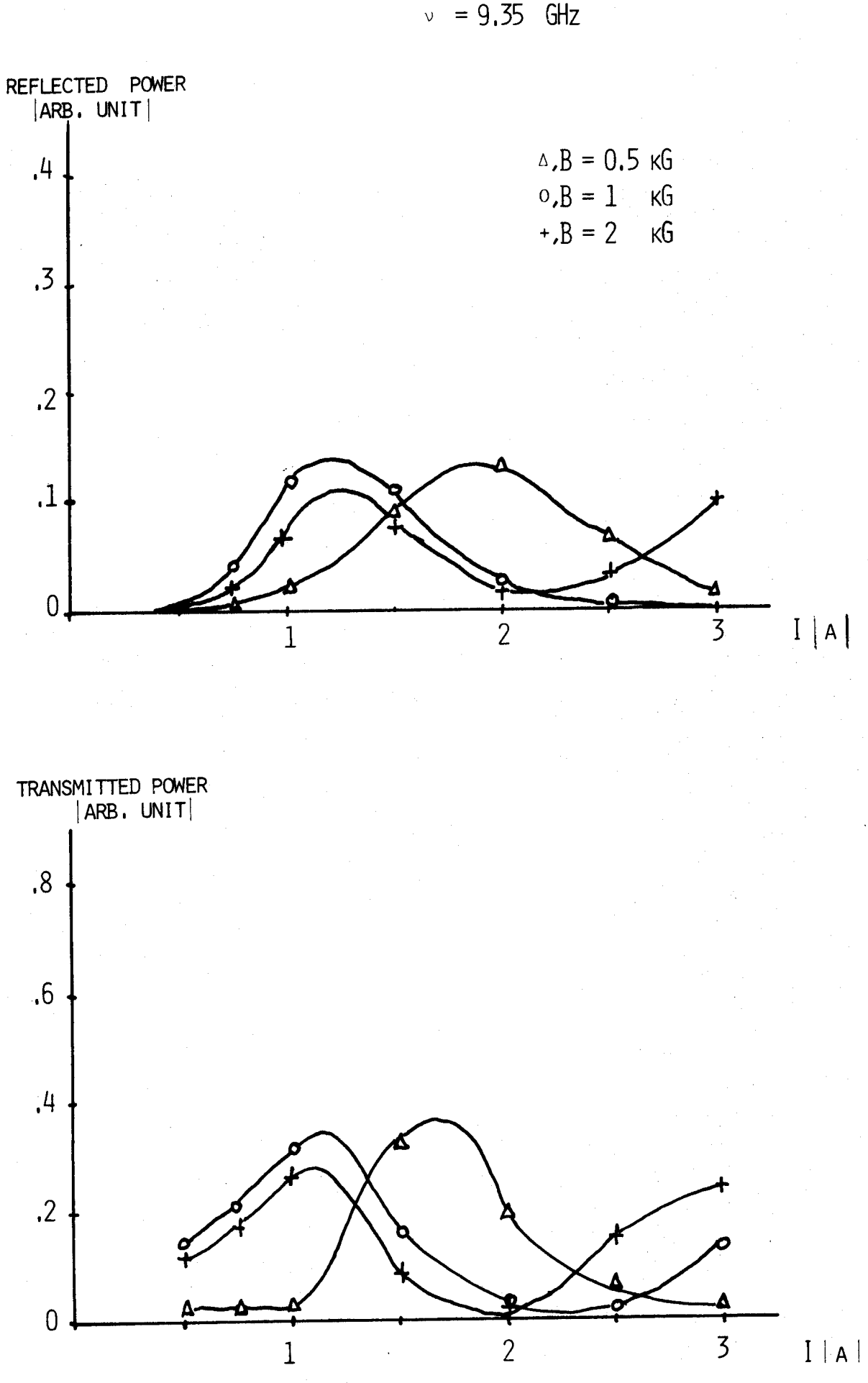
ν = 9.35 GHz
REFLECTED POWER
|ARB. UNIT|
Δ,B = 0.5 KG
o,B = 1 KG
+,B = 2 KG
.4
.3
.2
.1
0
1
2
3
I |A|
TRANSMITTED POWER
|ARB. UNIT|
.8
.6
.4
.2
0
1
2
3
I |A|

FIG 13

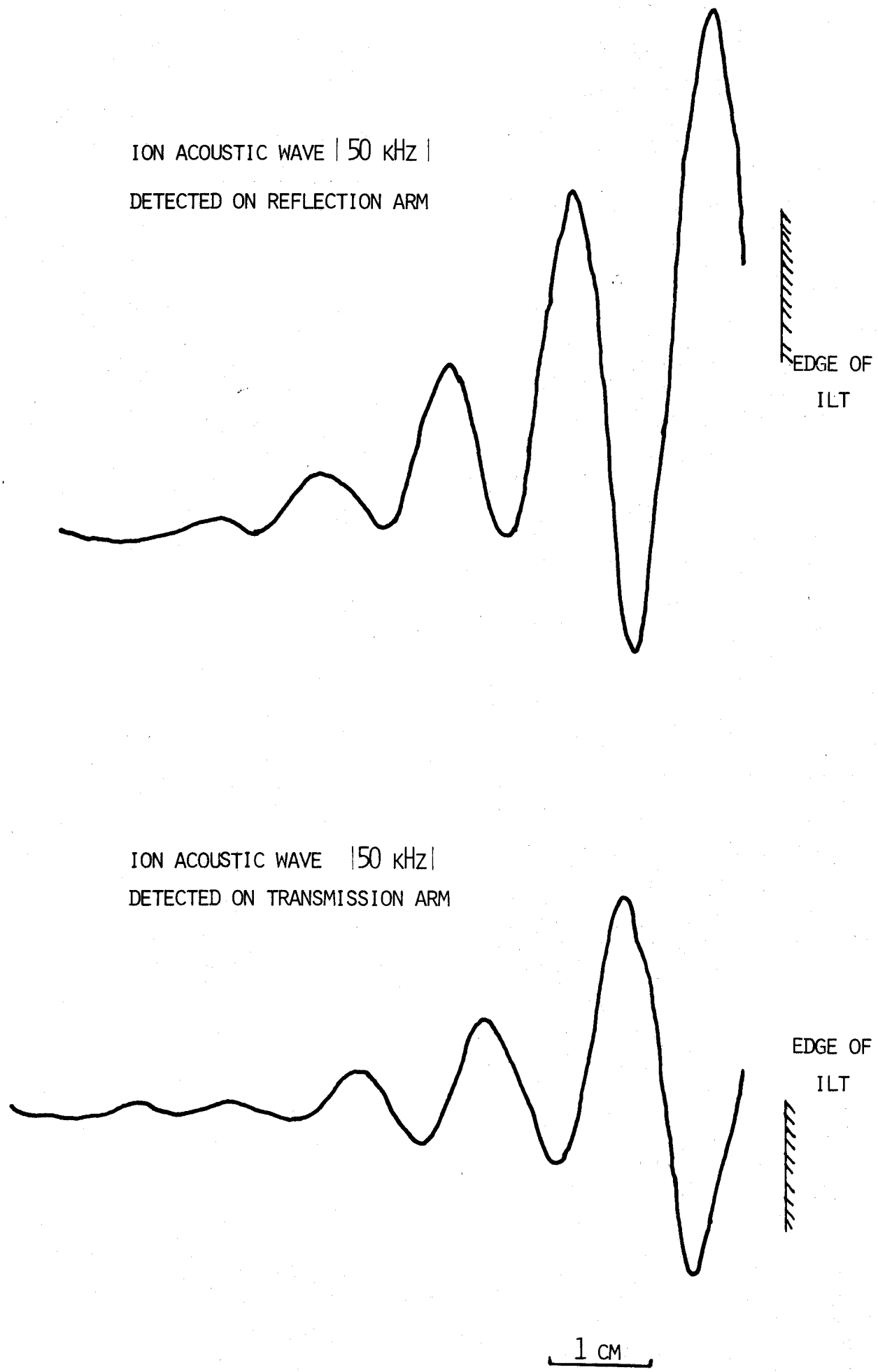
ION ACOUSTIC WAVE | 50 KHz |
DETECTED ON REFLECTION ARM
EDGE OF
ILT
ION ACOUSTIC WAVE |50 KHz|
DETECTED ON TRANSMISSION ARM
EDGE OF
ILT
1 CM

FIG 14

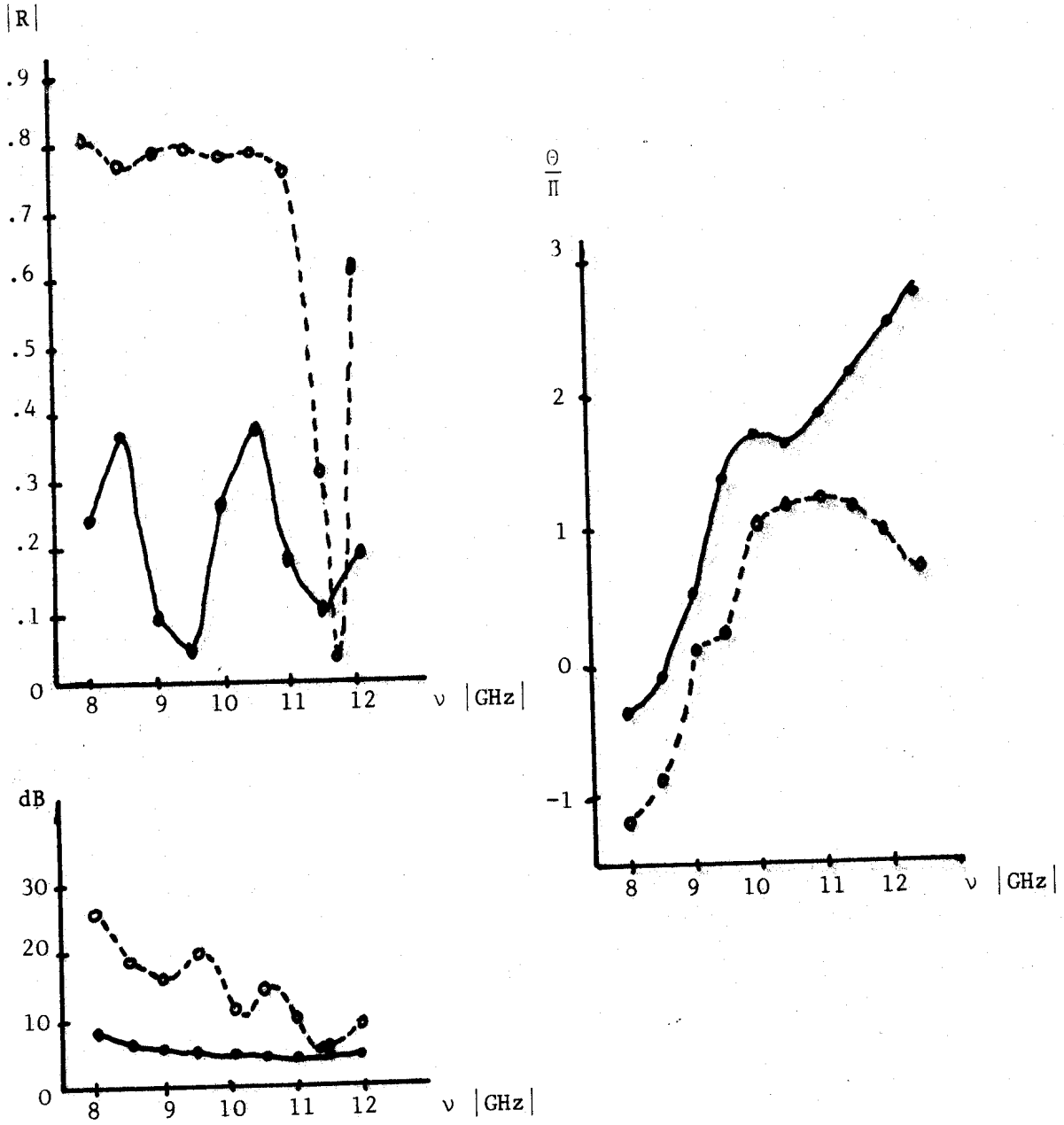

Reflection, attenuation and reflection Phase coefficients versus frequency for IST Set-up

FIG 15

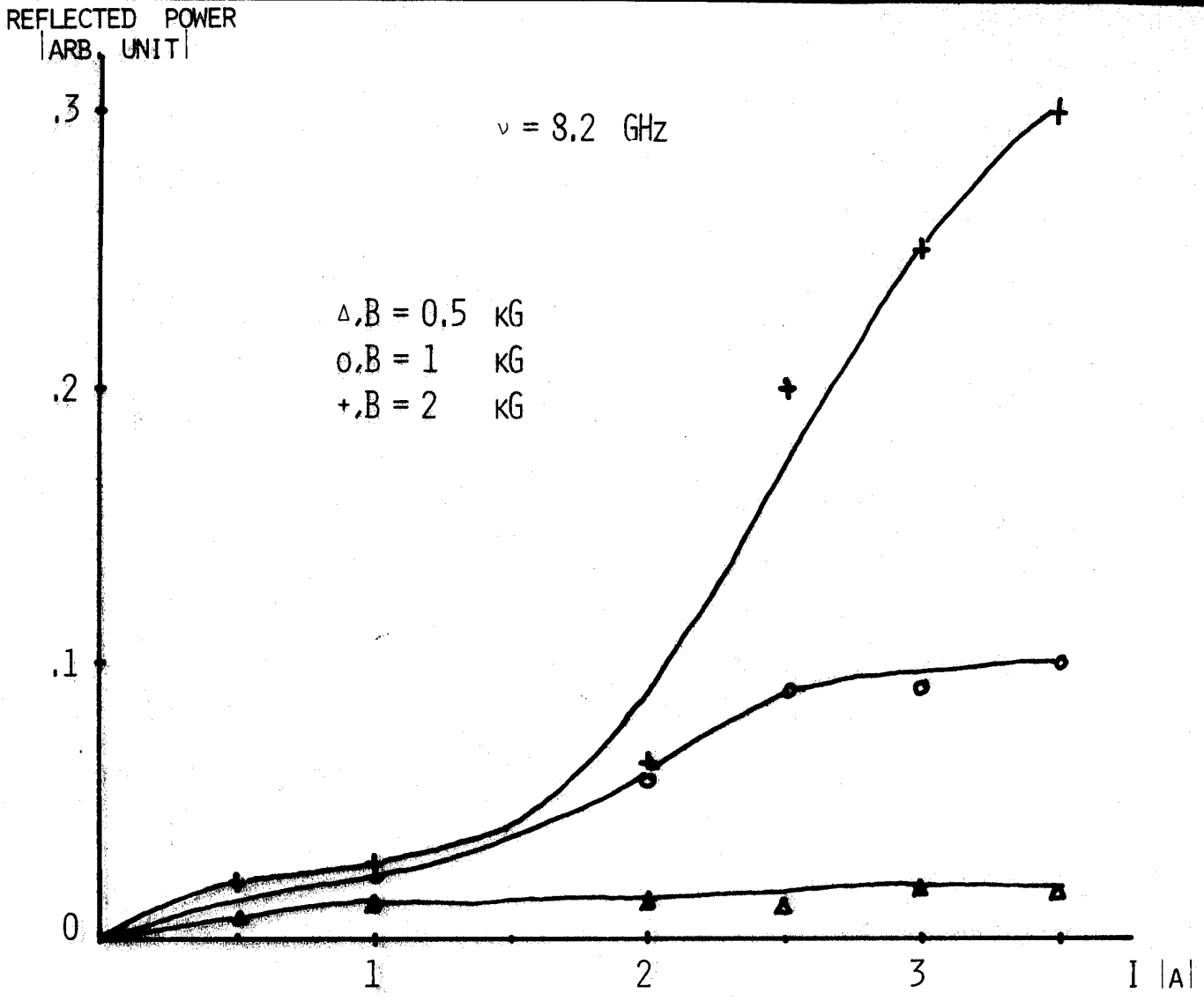
REFLECTED POWER
ARB. UNIT
.3
.2
.1
0
ν = 8.2 GHz
Δ, B = 0.5 KG
o, B = 1 KG
+, B = 2 KG
1
2
3
I |A|

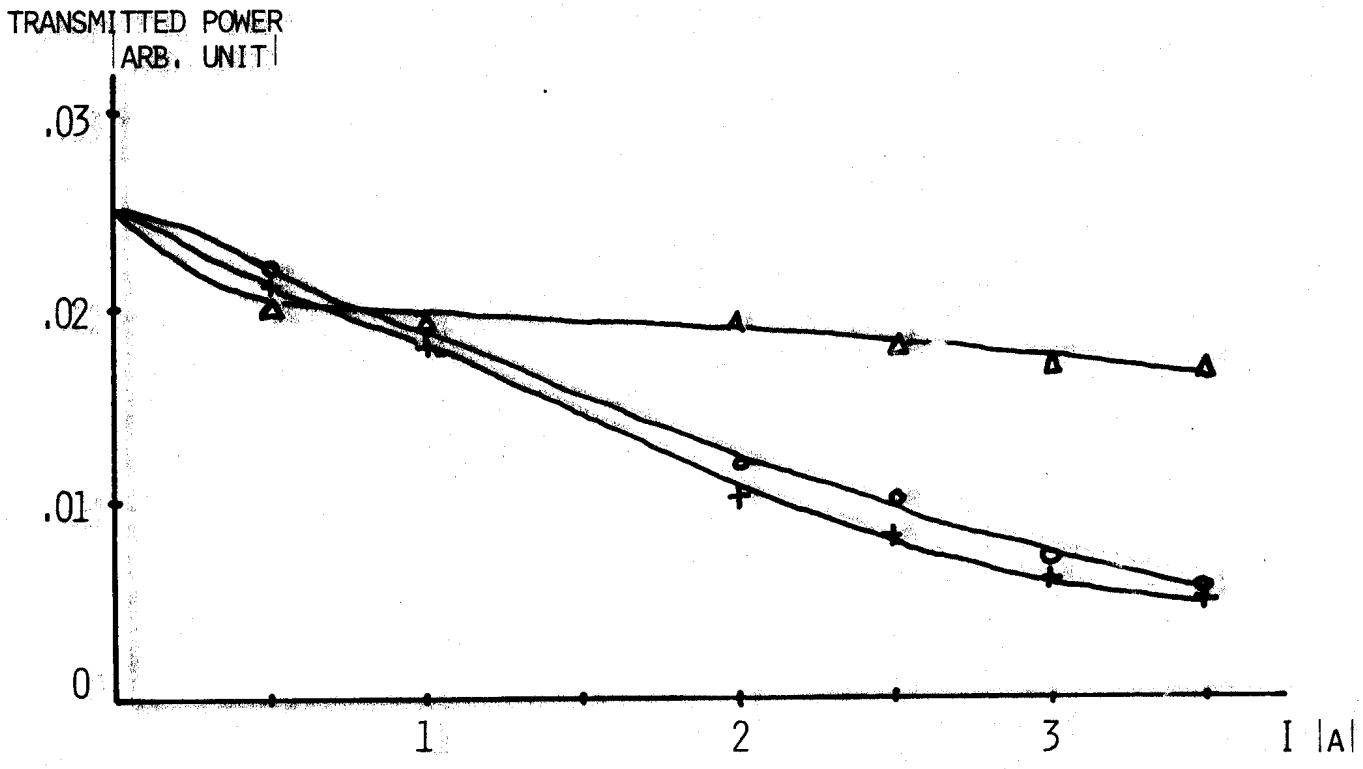
TRANSMITTED POWER
ARB. UNIT
.03
.02
.01
0
1
2
3
I |A|

FIG. 16

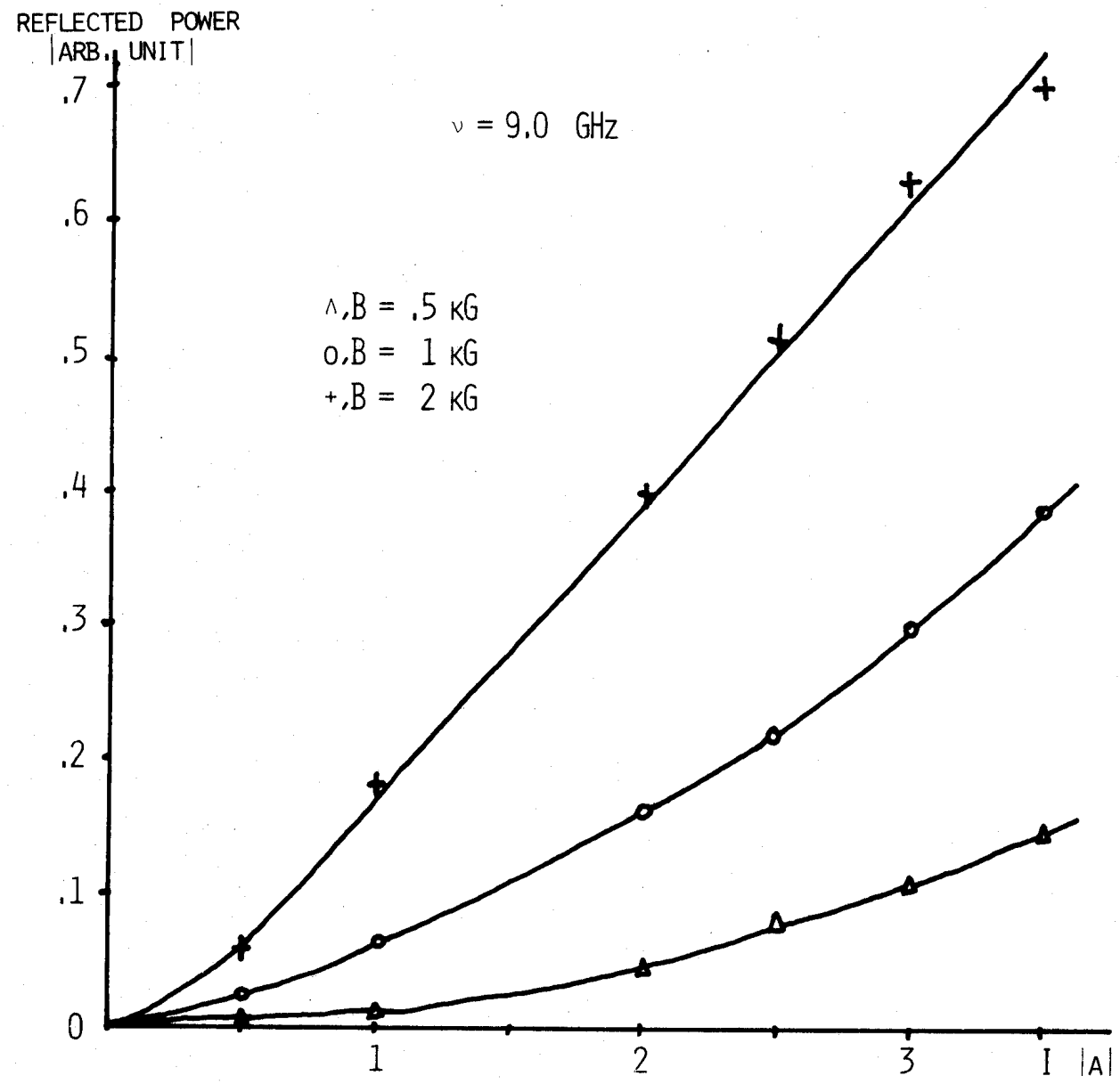
REFLECTED POWER
|ARB. UNIT|
.7
.6
.5
.4
.3
.2
.1
0
ν = 9.0 GHz
∧,B = .5 KG
o,B = 1 KG
+,B = 2 KG
1
2
3
I |A|

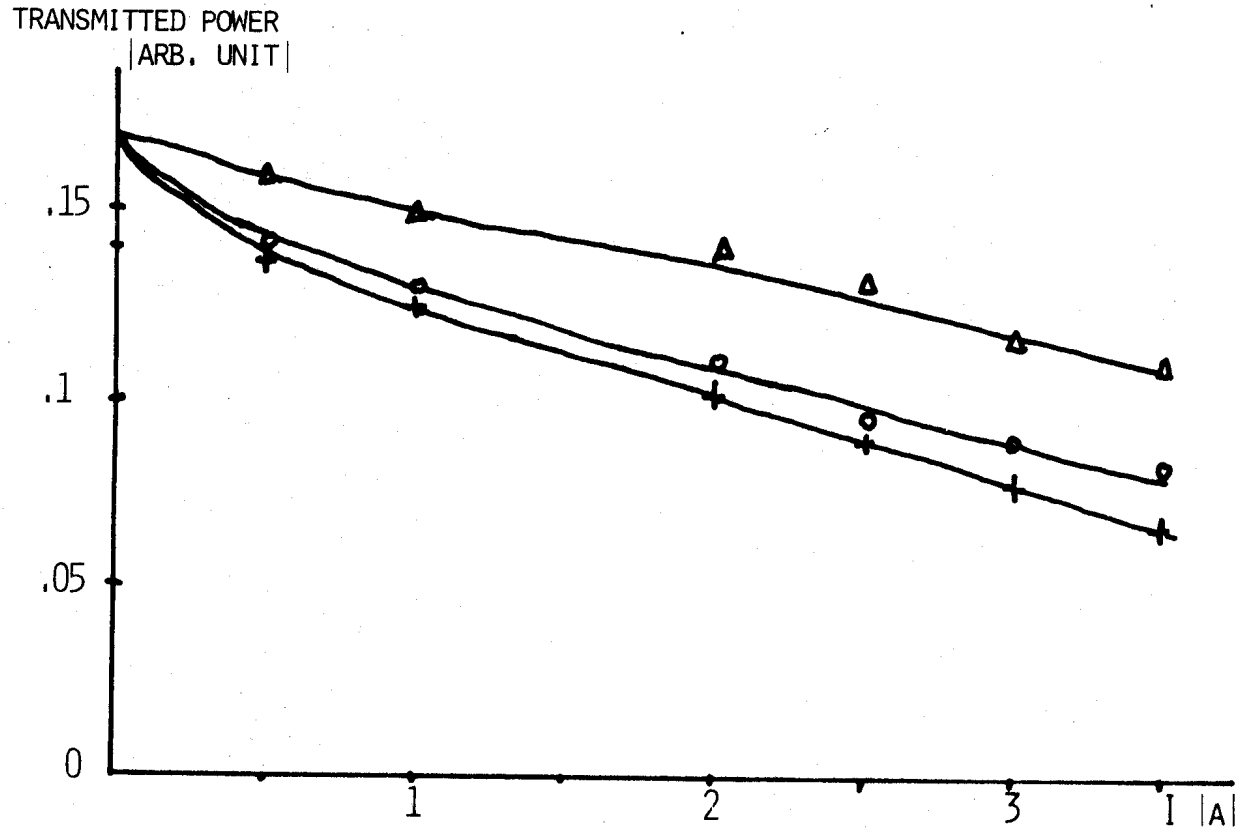
TRANSMITTED POWER
|ARB. UNIT|
.15
.1
.05
0
1
2
3
I |A|

FIG 17

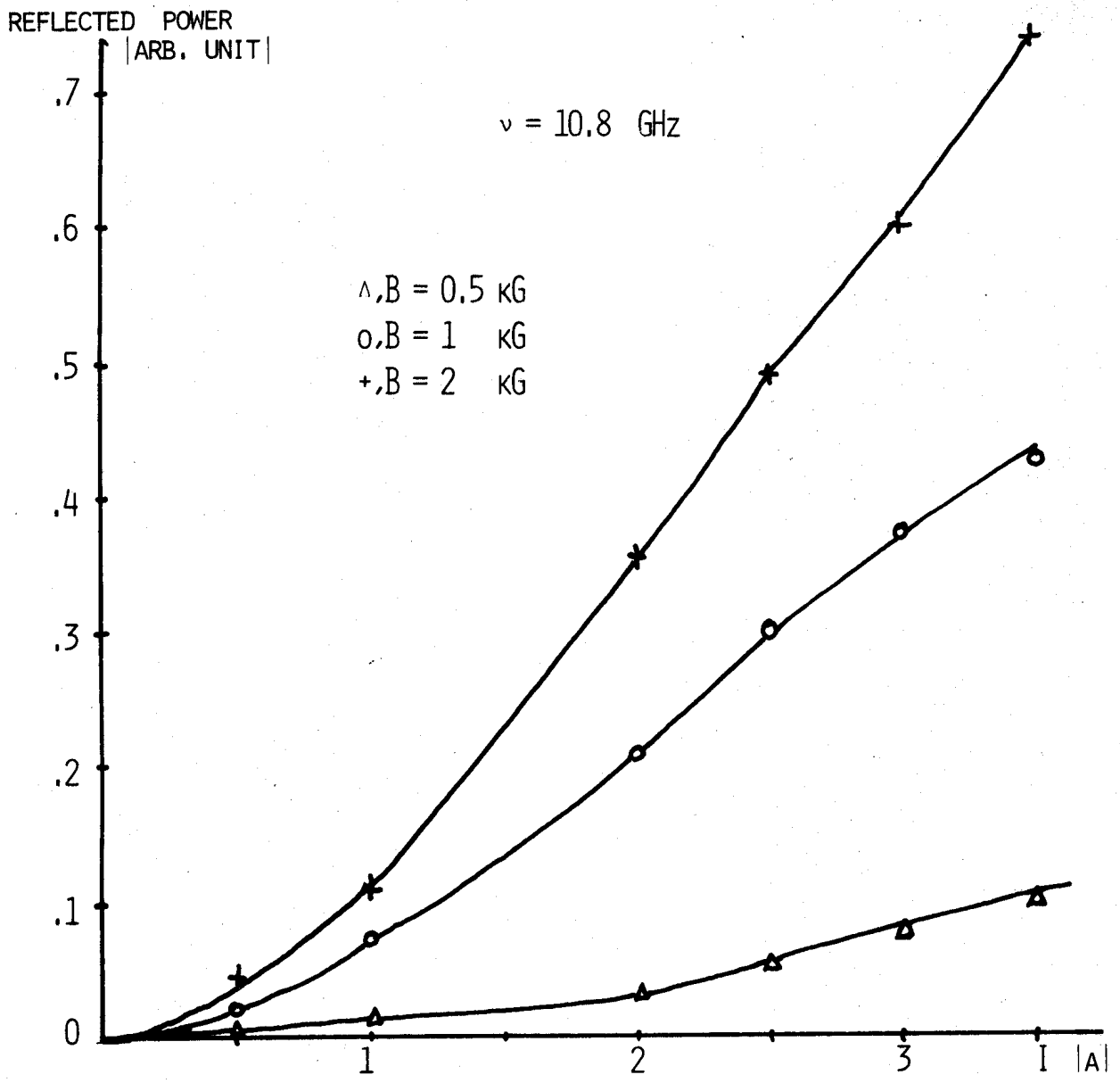
REFLECTED POWER
|ARB. UNIT|
.7
.6
.5
.4
.3
.2
.1
0
ν = 10.8 GHz
∧,B = 0.5 KG
o,B = 1 KG
+,B = 2 KG
1
2
3
I |A|

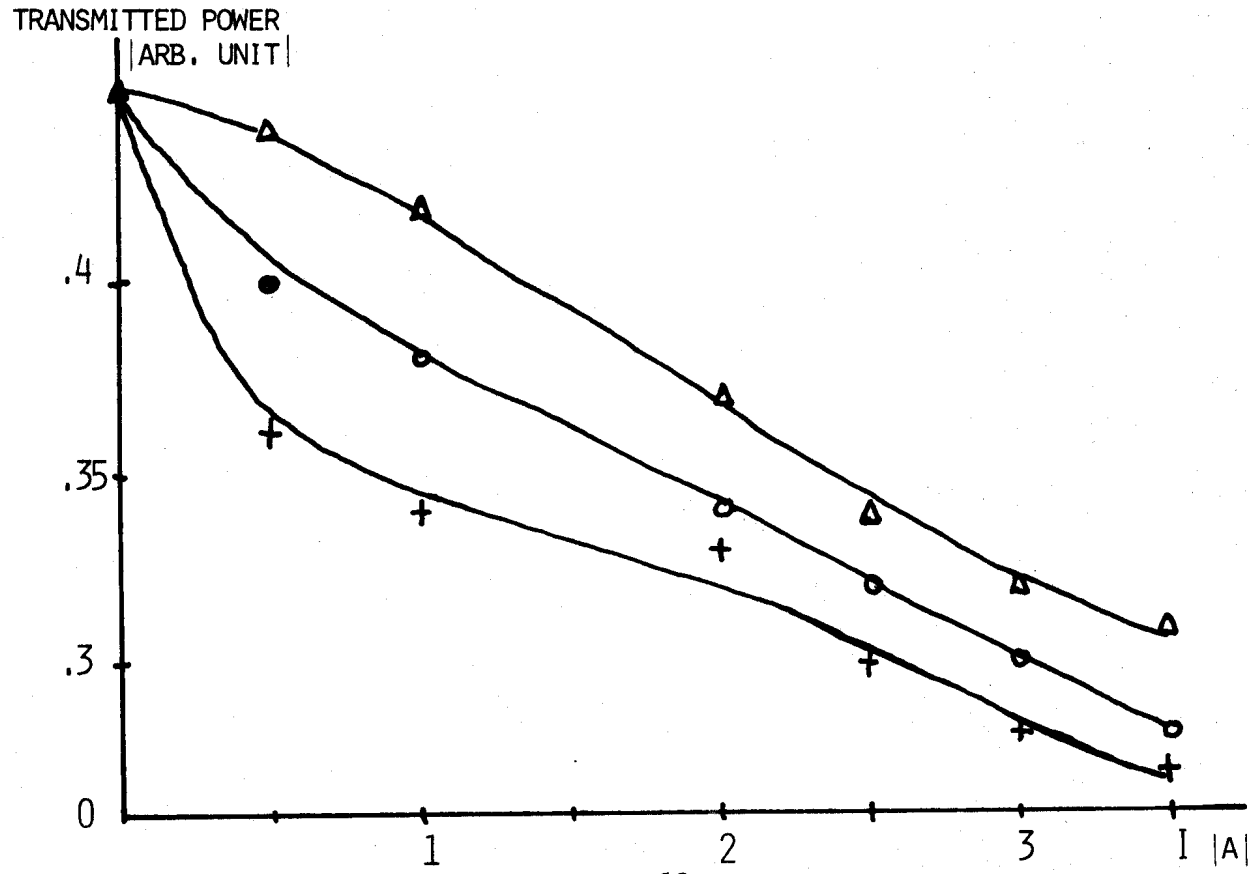
TRANSMITTED POWER
|ARB. UNIT|
.4
.35
.3
0
1
2
3
I |A|

FIG 18

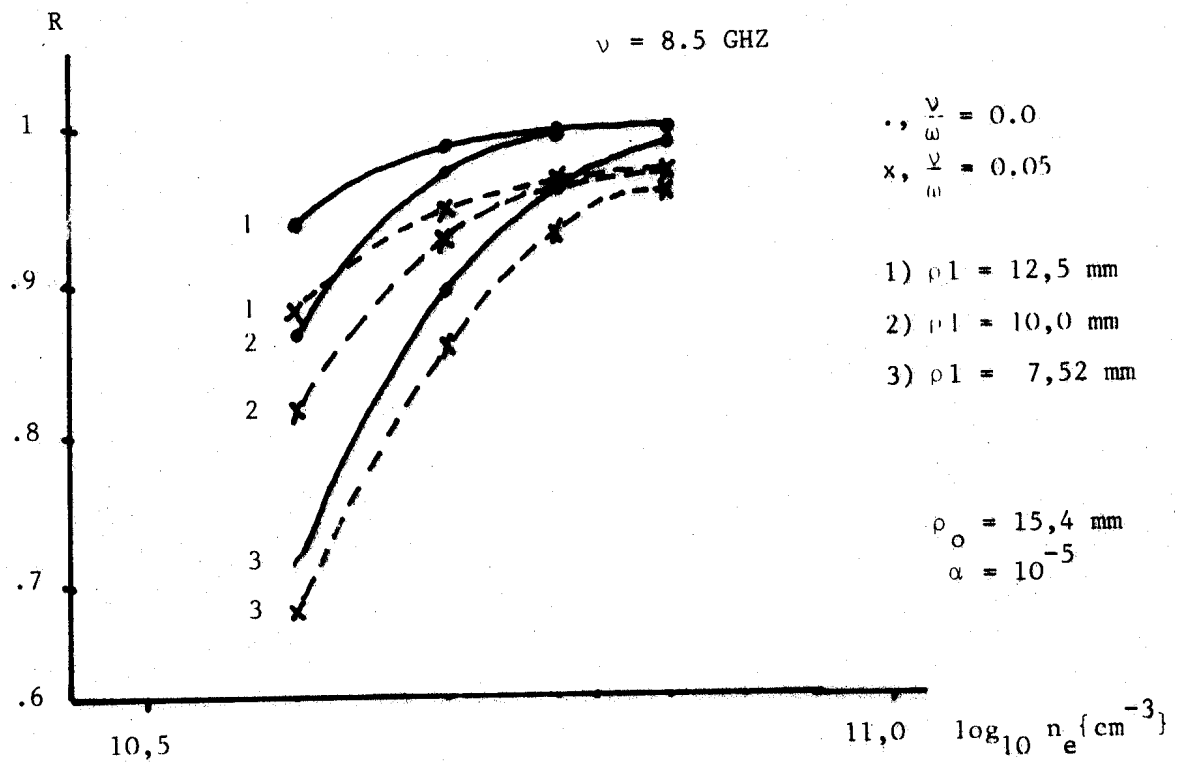
R
ν = 8.5 GHZ
1
.9
.8
.7
.6
10,5
11,0
log10 ne{cm-3}
., ν/ω = 0.0
x, ν/ω = 0.05
1) ρ1 = 12,5 mm
2) ρ1 = 10,0 mm
3) ρ1 = 7,52 mm
ρo = 15,4 mm
α = 10-5

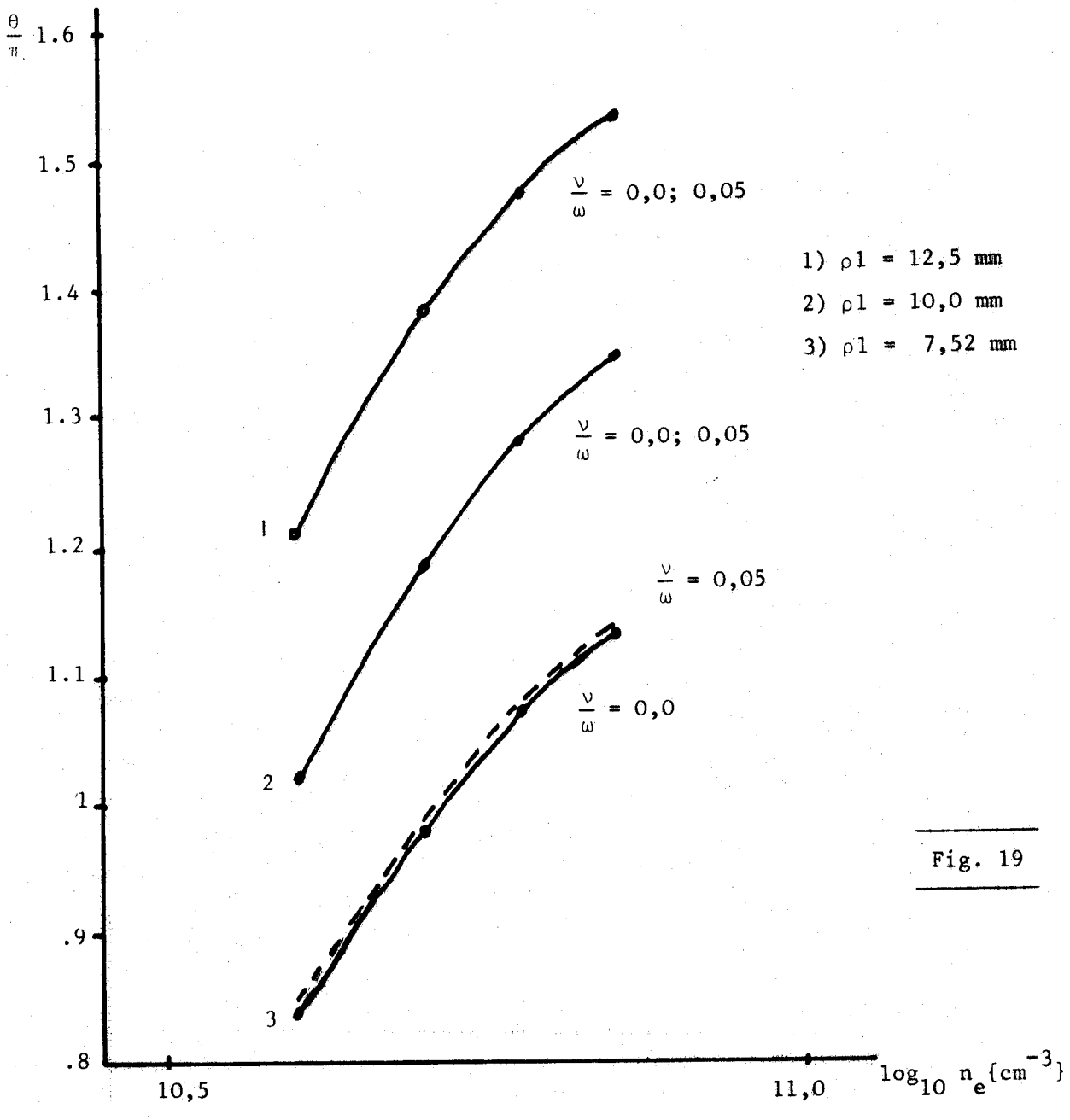
θ/π
1.6
1.5
1.4
1.3
1.2
1.1
1
.9
.8
10,5
11,0
log10 ne{cm-3}
ν/ω = 0,0; 0,05
ν/ω = 0,0; 0,05
ν/ω = 0,05
ν/ω = 0,0
1) ρ1 = 12,5 mm
2) ρ1 = 10,0 mm
3) ρ1 = 7,52 mm

Fig. 19

THEORETICAL CURVES AND MEASUREMENTS

- REFLEX CODE WAS APPLIED -

ILT

ν = 8.15 GHz K = 170 M^{-1}

K_ρ = 4.0 ρ = 23.6 MM $\left|\frac{\nu}{\omega} = 0.0\right.$

K_ρ = 3.0 ρ = 17.6 MM $\left|\frac{\nu}{\omega} = 0.0\right.$

▲ , B = 0.5 KG

\+ , B = 2 KG

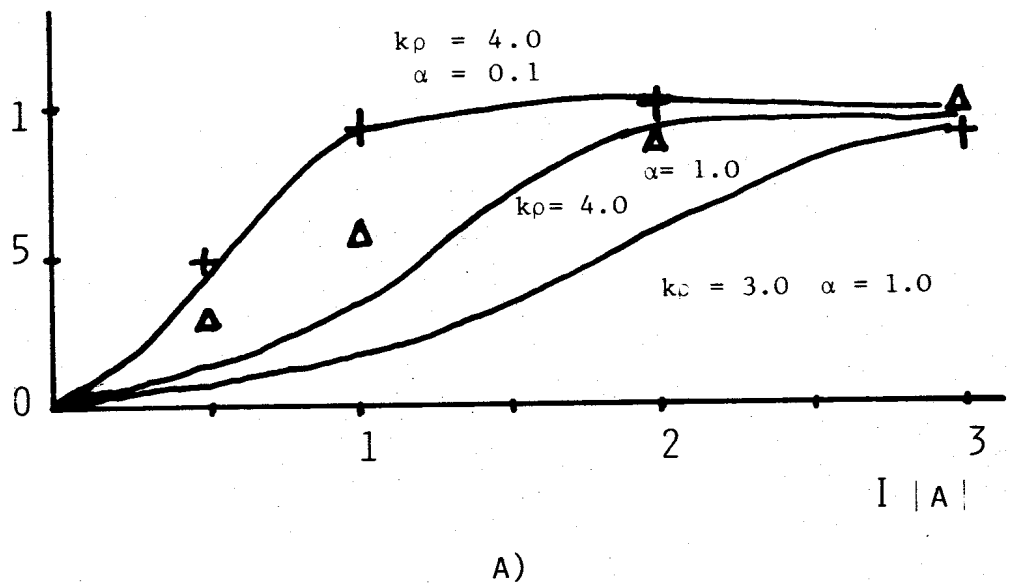

A)

IST

ν = 9.0 GHz K = 188 M^{-1}

K_ρ = 1.88 ρ = 10 MM

\+ , B = 2 KG

○ , B = 1 KG

▲ , B = 0.5 KG

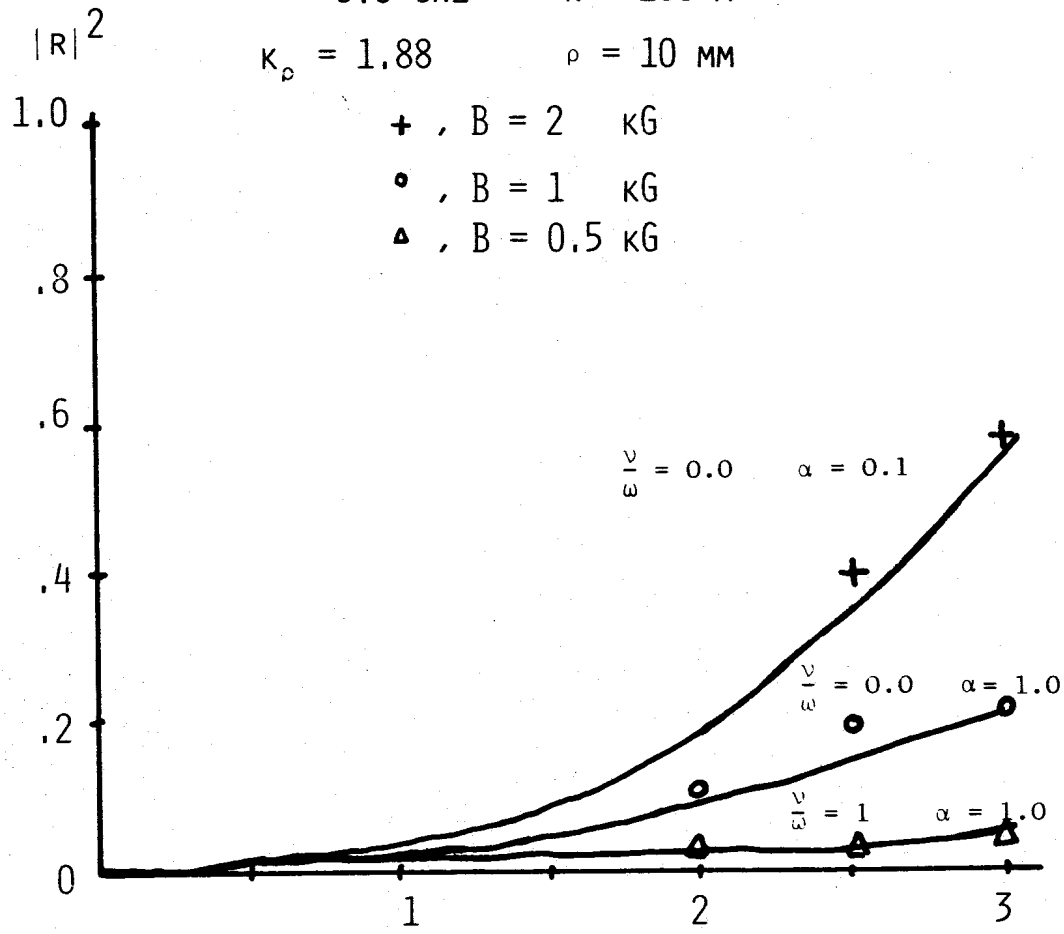

B)

FIG 20